

From Symmetry to Geometry: Tractable Nonconvex Problems

Yuqian Zhang[#], Qing Qu[◇], and John Wright^{†‡}

[#]Department of Electrical & Computer Engineering, Rutgers University

[◇]Department of Electrical Engineering and Computer Science, University of Michigan

[†]Department of Electrical Engineering and Data Science Institute, Columbia University

[‡]Department of Applied Physics and Applied Mathematics, Columbia University

Abstract

As science and engineering have become increasingly data-driven, the role of optimization has expanded to touch almost every stage of the data analysis pipeline, from signal and data acquisition to modeling and prediction. The optimization problems encountered in practice are often nonconvex. While challenges vary from problem to problem, one common source of nonconvexity is *nonlinearity* in the data or measurement model. Nonlinear models often exhibit *symmetries*, creating complicated, nonconvex objective landscapes, with multiple equivalent solutions. Nevertheless, simple methods (e.g., gradient descent) often perform surprisingly well in practice.

The goal of this survey is to highlight a class of tractable nonconvex problems, which can be understood through the lens of symmetries. These problems exhibit a characteristic geometric structure: local minimizers are symmetric copies of a single “ground truth” solution, while other critical points occur at balanced superpositions of symmetric copies of the ground truth, and exhibit negative curvature in directions that break the symmetry. This structure enables efficient methods to obtain global minimizers. We discuss examples of this phenomenon arising from a wide range of problems in imaging, signal processing, and data analysis. We highlight the key role of symmetry in shaping the objective landscape and discuss the different roles of rotational and discrete symmetries. This area is rich with observed phenomena and open problems; we close by highlighting directions for future research.

Contents

1	Introduction	2
2	Nonconvex Problems with Rotational Symmetry	7
2.1	One Minimal Example: Phase Retrieval with a Single Unknown	7
2.2	Generalized Phase Retrieval	8
2.3	Low Rank Matrix Recovery	11
3	Nonconvex Problems with Discrete Symmetry	15
3.1	Minimal Example: Dictionary Learning with One-Sparse Data	15
3.2	Dictionary Learning	17
3.3	Sparse Blind Deconvolution	18
3.4	Other Nonconvex Problems with Discrete Symmetry	20
4	Discussion	21
4.1	Symmetry & Geometry in Training Deep Neural Networks	21
4.2	Methodological Points & Future Directions	23
A	Critical Points of Low Rank Matrix Factorization	36

arXiv:2007.06753v4 [cs.LG] 8 Jul 2022

1 Introduction

As engineering and the sciences become increasingly data and computation driven, the role of optimization has expanded to touch almost every stage of the data analysis pipeline, from the signal and data acquisition to modeling and prediction. While the challenges in computing with physical data are many and varied, basic recurring issues arise from *nonlinearities* at different stages of this pipeline:

- **Nonlinear measurements** are ubiquitous in imaging, optics, and astronomy. A canonical example is sensing magnitude measurements, which arises when it is easy to measure the (Fourier) modulus of a complex signal, but hard to measure the phase. For example, we might measure the Fourier magnitude of a complex signal $\mathbf{x} \in \mathbb{C}^n$ [1–4]

$$\underset{\text{observation}}{\mathbf{y}} = \left| \mathcal{F} \left(\underset{\text{unknown signal}}{\mathbf{x}} \right) \right| \in \mathbb{R}^m. \quad (1.1)$$

Here, $\mathcal{F}(\cdot)$ denotes the Fourier transform, \mathbf{x} represents a signal or image of interest, and the goal is to reconstruct \mathbf{x} from the nonlinear measurements \mathbf{y} .

- **Nonlinear models** are often well-suited to express the variability of real datasets. For example, observations in microscopy, neuroscience, and astronomy can often be approximated as sparse superpositions of basic motifs. We can cast the problem of finding these motifs as one of seeking a representation of the form

$$\underset{\text{data}}{\mathbf{Y}} = \underset{\text{motifs}}{\mathbf{A}} \underset{\text{sparse coefficients}}{\mathbf{X}}. \quad (1.2)$$

Here, the columns of $\mathbf{Y} \in \mathbb{R}^{m \times p}$ are observed data vectors, the columns of $\mathbf{A} \in \mathbb{R}^{m \times n}$ are basic motifs, and $\mathbf{X} \in \mathbb{R}^{n \times p}$ is a sparse matrix of coefficients that expresses each observed data point as a superposition of motifs. This is sometimes called a sparse dictionary model. A typical goal is to infer both \mathbf{A} and \mathbf{X} from observed data. Because both \mathbf{A} and \mathbf{X} are unknown, this model should be considered nonlinear (strictly, bilinear). Natural images may have even more variability, which is better modeled by hierarchical models (convolutional neural networks) with more complicated nonlinearities [5–7].

Nonlinearity, Symmetry, and Nonconvexity In the examples described above, nonlinearities are not just a nuisance: they have strong implications on the sense in which we can hope to solve these problems, and, as we shall see in this paper, on our ability to efficiently compute solutions. Both above models exhibit *symmetries*. The model $\mathbf{y} = |\mathcal{F}(\mathbf{x})|$ in (1.1) exhibits a *phase symmetry*: both \mathbf{x} and $\mathbf{x}e^{i\phi}$ (for any $\phi \in [0, 2\pi)$) produce the same observation \mathbf{y} . The sparse dictionary model $\mathbf{Y} = \mathbf{A}\mathbf{X}$ exhibits a *permutation symmetry*: for any permutation $\mathbf{\Pi}$, (\mathbf{A}, \mathbf{X}) and $(\mathbf{A}\mathbf{\Pi}, \mathbf{\Pi}^*\mathbf{X})$ produce the same observation \mathbf{Y} .¹

In either case, we can only hope to recover the physical ground-truth up to these basic symmetries. A typical computational approach is to formulate it as an optimization problem

$$\min_{\mathbf{z}} \varphi(\mathbf{z}), \quad (1.3)$$

and attempt to solve it with iterative methods such as gradient descent [8]. Here, \mathbf{z} represents the signal or model to be recovered – for example, in phase retrieval, $\mathbf{z} = \mathbf{x}$, while in dictionary learning the optimization variable \mathbf{z} is the pair (\mathbf{A}, \mathbf{X}) . Typically, $\varphi(\cdot)$ measures quality of fit to observed data and the extent to which the solution satisfies assumptions such as sparsity. As we shall see, most natural choices of $\varphi(\cdot)$ inherit the symmetries of the data generation model: e.g., for phase recovery, we have $\varphi(e^{i\theta}\mathbf{x}) = \varphi(\mathbf{x})$, while for dictionary learning, $\varphi((\mathbf{A}, \mathbf{X})) = \varphi((\mathbf{A}\mathbf{\Pi}, \mathbf{\Pi}^*\mathbf{X}))$: *symmetries of the observation models become symmetries of the optimization problem*.

If we are judicious in our choice of $\varphi(\cdot)$, we can hope that the true \mathbf{x} is a (near) global minimizer; our task becomes solving the optimization problem (1.3) to the global optimality. In contrast to certain applications

¹Here, and throughout the paper, the notation M^* denotes the complex conjugate transpose of a matrix M . If M is real-valued, this is simply the matrix transpose.

of numerical optimization (e.g., in finance, logistics, deep learning, etc.), we care not just about decreasing the objective function, but about obtaining the physical ground truth. As such, we are forced to care not just about ensuring that our algorithms converge, but that they converge to the global minimizers. In applied optimization, a time-honored approach for guaranteeing global optimality is to seek formulations that are convex. The global minimizers of a convex function form a convex set. Moreover, every local minimizer (indeed, every critical point) of a convex function is global. As a result, many convex problems can be efficiently solved to global optimality by local methods. This makes the area of convex analysis and optimization a model for how geometric understanding can support practical computations.

Unfortunately, as alluded to above, the symmetric problems we encounter in statistics, signal processing, and related areas are typically nonconvex [9–12], and so we need to look for other geometric principles that will enable us to guarantee high-quality solutions. Indeed, these problems exhibit multiple global minimizers, which may be disjoint (due to permutation symmetry) or may reside on a nonconvex set (due to rotation or phase symmetry). Any optimization formulation that inherits these symmetries will be nonconvex.²

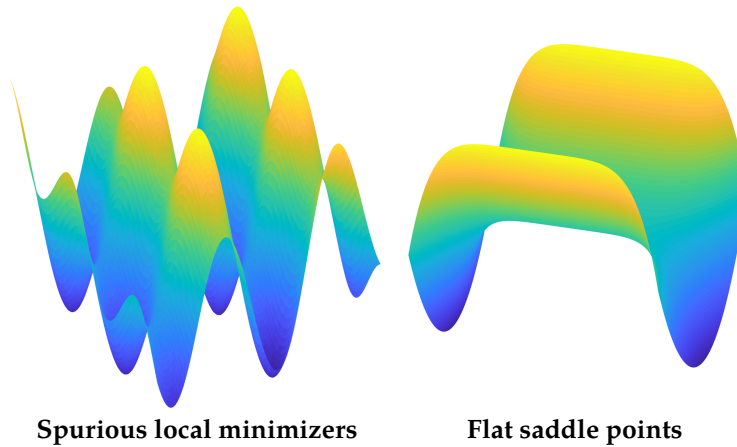


Figure 1: Two geometric obstructions to nonconvex optimization. Local methods can become trapped near local minimizers (left) or stagnate near flat saddle points (right).

Worst Case Obstructions to Nonconvex Optimization This observation might suggest a certain pessimism: *nonconvex optimization is impossible in general*. There are simple classes of nonconvex problems (e.g., in polynomial optimization) that are NP-hard [13]. At a more intuitive level, there are two geometric obstructions to solving nonconvex problems globally. First, nonconvex problems can exhibit *spurious local minimizers*, i.e. local minimizers that are not global (see Figure 1 (left) for an illustration). Local descent methods can get trapped; finding the global optimum is hard in general. Perhaps surprisingly, even finding a *local* minimizer is NP-hard in general [13, 14]. Figure 1 (right) illustrates the challenge: it is possible to construct objective functions that are so flat that it is impossible to efficiently determine a descent direction.

Calculus and the Local Geometry of Optimization Because of these worst case obstructions, the classical literature on efficient³ nonconvex optimization has focused on guaranteeing

- (i) convergence to some critical point (\bar{z} such that $\nabla\varphi(\bar{z}) = \mathbf{0}$),
- (ii) or convergence to some local minimizers, for functions $\varphi(\cdot)$ which are not too flat.

²**Disclaimer:** Not *every* symmetric problem is nonconvex. Indeed, the objective function $\varphi(\mathbf{z}) = \frac{1}{2}\|\mathbf{z}\|_2^2$ is rotationally symmetric $\varphi(\mathbf{Rz}) = \varphi(\mathbf{z})$ for all $\mathbf{R} \in O(n)$, $\mathbf{z} \in \mathbb{R}^n$ and convex. It is easy to construct additional examples of this type. However, the symmetric problems encountered in statistics, signal processing, and related areas are typically nonconvex; moreover, their nonconvexity can be directly attributed to symmetry.

³Of course, it is also possible to find global optima under minimal assumptions by exhaustively exploring the space of optimization, e.g., by discretization [15] or by random search [16, 17]. The worst case obstructions described above still rear their heads, in the form of search times that are exponential in dimension.

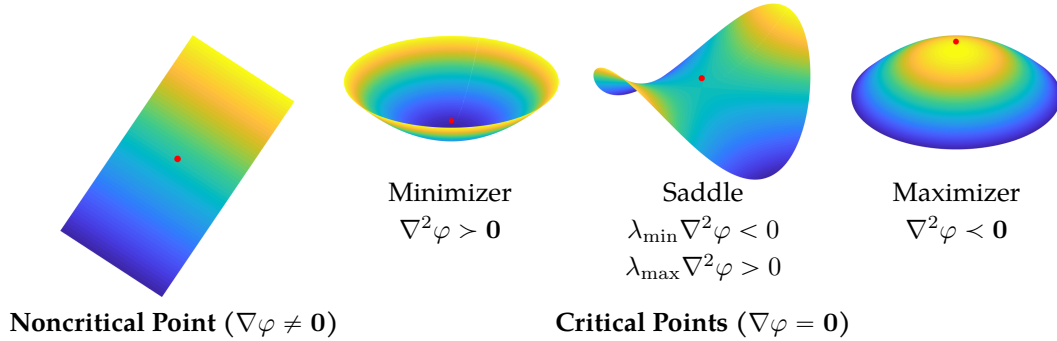


Figure 2: Calculus and the local geometry of optimization. The *gradient* $\nabla\varphi$ captures the slope of the function φ . At *critical points* \bar{z} , $\nabla\varphi(\bar{z}) = \mathbf{0}$. The type of critical point (minimizer, maximizer, saddle) can often be determined from the curvature of φ at \bar{z} , which is captured by the *Hessian* $\nabla^2\varphi(\bar{z})$.

The curvature of a smooth function $\varphi(\cdot)$ around a critical point \bar{z} can be studied through the Hessian $\nabla^2\varphi(\bar{z})$. If $\nabla^2\varphi(\bar{z})$ is nonsingular, the signs of its eigenvalues completely determine whether \bar{z} is a minimizer, maximizer, or saddle point – see Figure 2 (right). In particular, if \bar{z} is a saddle point or a minimizer, there is a direction of negative curvature – a direction along which the second derivative is negative. This information can be used to escape saddles and converge to a local minimizer, either explicitly (using the Hessian [18–20]) or implicitly (using gradient information [21–23]). There are a variety of iterative methods that trade-off in various ways between the amount of computation used to determine a good direction of negative curvature at a given iteration and the number of iterations required to converge [19, 21, 24–27]. However, the high-level message of these methods is consistent: if all critical points are nondegenerate,⁴ we can escape them and efficiently converge to a local minimizer. In fact, slightly less is required: it is enough that every non-minimizing critical point have a direction of strict negative curvature [21, 26, 30, 31].⁵

Results of this nature control the worst-case behavior of optimization methods over very broad classes of problems. In such a general setting, it is impossible to provide strong guarantees on *what* local minimizer that optimization methods converge to, and whether that minimizer is global. Nevertheless, it is difficult to overstate the impact of this kind of thinking for stimulating the development of useful methods and elucidating their properties. Moreover, optimization methods developed to guarantee good worst-case performance often outperform their worst-case guarantees on practical problem instances – we witnessed longstanding “folk theorems” on the ease of optimizing neural networks [32–37], solving problems in quantum mechanics [38–40] or clustering separated data [41–44]. Delineating problem classes that capture the difficulty (or ease!) of naturally occurring nonconvex optimization problems is a pressing challenge for the mathematics of data science [9–12].

Symmetry and the Global Geometry of Optimization? The goal of this survey paper is to highlight a particular family of easy nonconvex problems which, under certain hypotheses, can be solved globally with efficient optimization methods. This family includes a number of contemporary problems in signal processing, data analysis, and related fields [9–12]. The most important high-level property of these problems is that they are *symmetric* – in slightly more formal mathematical language:

Definition 1.1 (Symmetric Function) Let \mathbb{G} be a group acting on \mathbb{R}^n . A function $\varphi : \mathbb{R}^n \rightarrow \mathbb{R}^n$ is \mathbb{G} -symmetric if for all $z \in \mathbb{R}^n$, $g \in \mathbb{G}$, $\varphi(g \cdot z) = \varphi(z)$.

As argued above, symmetry forces us to grapple with the properties of nonconvex functions. On the other hand, the particular symmetric nonconvex functions encountered in practice are often quite benign. Figure 3 shows two examples – one with rotational symmetry (e.g., \mathbb{G} is an orthogonal group) and one with discrete symmetry (e.g., \mathbb{G} is a discrete group, such as signed permutations). We will develop these examples in more

⁴In the language of topology, if the function φ is Morse [28, 29].

⁵In the recent literature, this is called a “strict saddle” property [9, 22]. Concrete rates of convergence are typically stated in terms of quantitative versions of this property, which explicitly control the size of the gradient and the smallest eigenvalue of the Hessian uniformly over the domain of optimization.

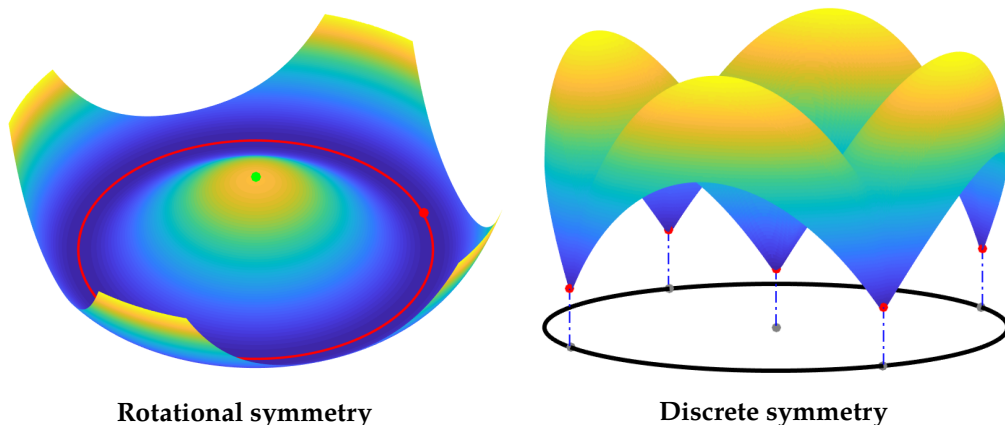


Figure 3: Symmetry and the global geometry of optimization. Model problems with continuous (left) and discrete (right) symmetry. For these particular problems, and a few others we will survey, every local minimizer is global.

mathematical detail below. For now, we simply observe that these two instances do not exhibit spurious local minimizers or flat saddle points. The absence of these worst-case obstructions can be attributed to benign symmetry structures. In slogan form, we shall see that:

Slogan I: *The (only!) local minimizers are symmetric versions of the ground truth.*

Slogan II: *There is negative curvature in directions that break symmetry.*

When these two slogans are in force, efficient (local) optimization methods produce global minimizers. Moreover, symmetry constrains the global layout of the critical points, leading to an additional structure that facilitates efficient optimization. We will show examples where the saddle points of symmetric problems “cascade”, with negative curvature directions feeding into other negative curvature directions subsequently, a benign property which appears to prevent first-order methods from stagnating [45].

Before we embark, a few disclaimers are in order. First, Slogans I and II are only slogans. As we shall see, they have been established rigorously for specific problems under specific (restrictive) technical hypotheses. We hope to convey a sense of the beauty and robustness of certain observed phenomena in optimization, while also making clear that the existing mathematics supporting these claims is in places ugly and brittle. There is a need for more unified analyses and better technical tools. We highlight some potential avenues for this in Section 4. The second, more fundamental, the disclaimer is that not all symmetric problems have benign global geometry. It is easy to construct counterexamples. Nevertheless, as we will see, symmetry provides a lens through which one can understand the geometric properties that enable efficient optimization for a particular family of problems. Moreover, when we study these problems through their symmetries, common structures and intuitions emerge: problems with similar symmetries exhibit similar geometric properties.

A Taxonomy of Symmetric Nonconvex Problems

In this paper, we identify two families of symmetric nonconvex problems, which exhibit similar geometric characteristics. The first family of problems exhibit *rotational symmetries*: the group \mathbb{G} is either an orthogonal group $O(n)$ or $SO(n)$.⁶ The phase retrieval problem described above is a canonical example; **Figure 4** illustrates this family. The second family of problems exhibit *discrete symmetries*: signed permutations $SP(n)$, signed shifts $\mathbb{Z}_n \times \{\pm 1\}$, or products of these. The dictionary learning problem discussed above is a canonical example; **Figure 5** shows several others.

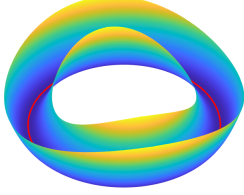
In the remainder of this paper, we explore the geometry of these two families of problems in more depth. Section 2 studies problems with rotational symmetries, starting with a very simple model problem in which the goal to recover a single complex scalar from magnitude measurements, and drawing conclusions that

⁶Here, $SO(n)$ is a subgroup of $O(n)$, with determinant equalling to unity.

Nonconvex Problems with Rotational Symmetries

Eigenspace Computation

Compute the principal subspace of a symmetric matrix.

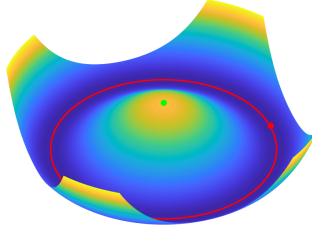


$$\min_{\mathbf{X}^* \mathbf{X} = \mathbf{I}} -\frac{1}{2} \text{trace}[\mathbf{X}^* \mathbf{A} \mathbf{X}].$$

Symmetry: $\mathbf{X} \mapsto \mathbf{X} \mathbf{R}$
 $\mathbb{G} = O(r)$

Generalized Phase Retrieval

Recover a complex vector \mathbf{x}_0 from magnitude measurements $\mathbf{y} = |\mathbf{A} \mathbf{x}_0|$.

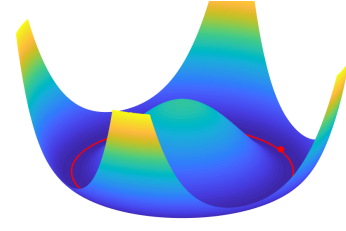


$$\min_{\mathbf{x}} \frac{1}{2} \|\mathbf{y}^2 - |\mathbf{A} \mathbf{x}|^2\|_2^2.$$

Symmetry: $\mathbf{x} \mapsto \mathbf{x} e^{i\phi}$
 $\mathbb{G} = \mathbb{S}^1 \cong O(2)$

Matrix Recovery

Recover a low-rank matrix $\mathbf{X} = \mathbf{U} \mathbf{V}^*$ from incomplete/corrupted observations



$$\min_{\mathbf{U}, \mathbf{V}} \mathcal{L}(\mathbf{Y} - \mathcal{A}[\mathbf{U} \mathbf{V}^*]) + \rho(\mathbf{U}, \mathbf{V}).$$

Symmetry: $(\mathbf{U}, \mathbf{V}) \mapsto (\mathbf{U} \mathbf{\Gamma}, \mathbf{V} \mathbf{\Gamma}^{-*})$
 $\mathbb{G} = \text{GL}(r)$ or $\mathbb{G} = O(r)$

Figure 4: Three examples of nonconvex optimization problems with rotational symmetries (Section 2). Each of these three tasks can be reduced to optimization problems in various ways; for each, we give a representative formulation and discuss its symmetries.

carry over to more complicated measurement models for phase retrieval [3, 46–49] and related problems in low-rank matrix factorization and recovery [11, 50, 51]. Section 3 studies problems with discrete symmetries, starting again from another simple model problem and extracting conclusions that carry over to problems such as dictionary learning [20, 45, 52, 53], blind deconvolution [54–59] and tensor decomposition [22, 60]. As mentioned above, this area is rich with open problems; we highlight a few of these in Section 4. These open problems span high-dimensional geometry and algorithms. Nevertheless, our main focus throughout this survey is geometric: we will concentrate on the connections between symmetry and geometry. As described above, these geometric analyses have strong implications: in many cases, they guarantee that problems can be solved globally in polynomial time. For problems with rotational symmetry, we recommend the (complementary) survey papers [23, 61, 62] for a more detailed exposition of issues at the interface of statistics and computation; Section 4 also briefly discusses similar considerations for problems exhibiting discrete symmetries, where we refer readers to our companion overview paper [63] for more computational and application aspects on these problems. On the other hand, in order to keep the development of this overview focused on geometric intuitions, we will only treat computational issues at a high level. For developments on 1st and 2nd order optimization methods related to this topic, we refer readers to recent works [10, 23, 64–67]. In particular, [10] focuses on alternating direction type of methods and local analysis for nonconvex optimization problems in machine learning; the recent works [23, 64, 66, 67] focus on reviews of efficient nonconvex optimization methods, including zero-th order [66], first-order [23] and second-order [66] methods, and Riemannian optimization methods [64, 65, 67]. As mentioned above, for many naturally occurring problems in signal processing and machine learning, these methods not only find critical points, they actually find global minimizers. The geometric considerations that we introduce below help explain why this is the case!

Basic notations. Before proceeding, we recap and introduce some basic notations. Throughout the paper, all vectors/matrices are written in bold font \mathbf{a}/\mathbf{A} ; indexed values are written as a_i, A_{ij} . For a matrix \mathbf{A} , we use \mathbf{A}^* to denote the transpose of \mathbf{A} (conjugate transpose if \mathbf{A} is complex). We use \mathbb{S}^{n-1} to denote an n -dimensional unit sphere in the Euclidean space \mathbb{R}^n . We let $[m] = \{1, 2, \dots, m\}$. We use \odot to denote the entry-wise Hadamard product, and we use $*$ to denote linear convolution. For any given vector \mathbf{a} , we use $\|\mathbf{a}\|_p = (\sum_{i=1}^n |a_i|^p)^{1/p}$ to denote its ℓ_p -norm. For any given matrix \mathbf{A} , we use $\|\mathbf{A}\|_F$ and $\|\mathbf{A}\|$ to denote its Frobenius norm and spectral norm, respectively.

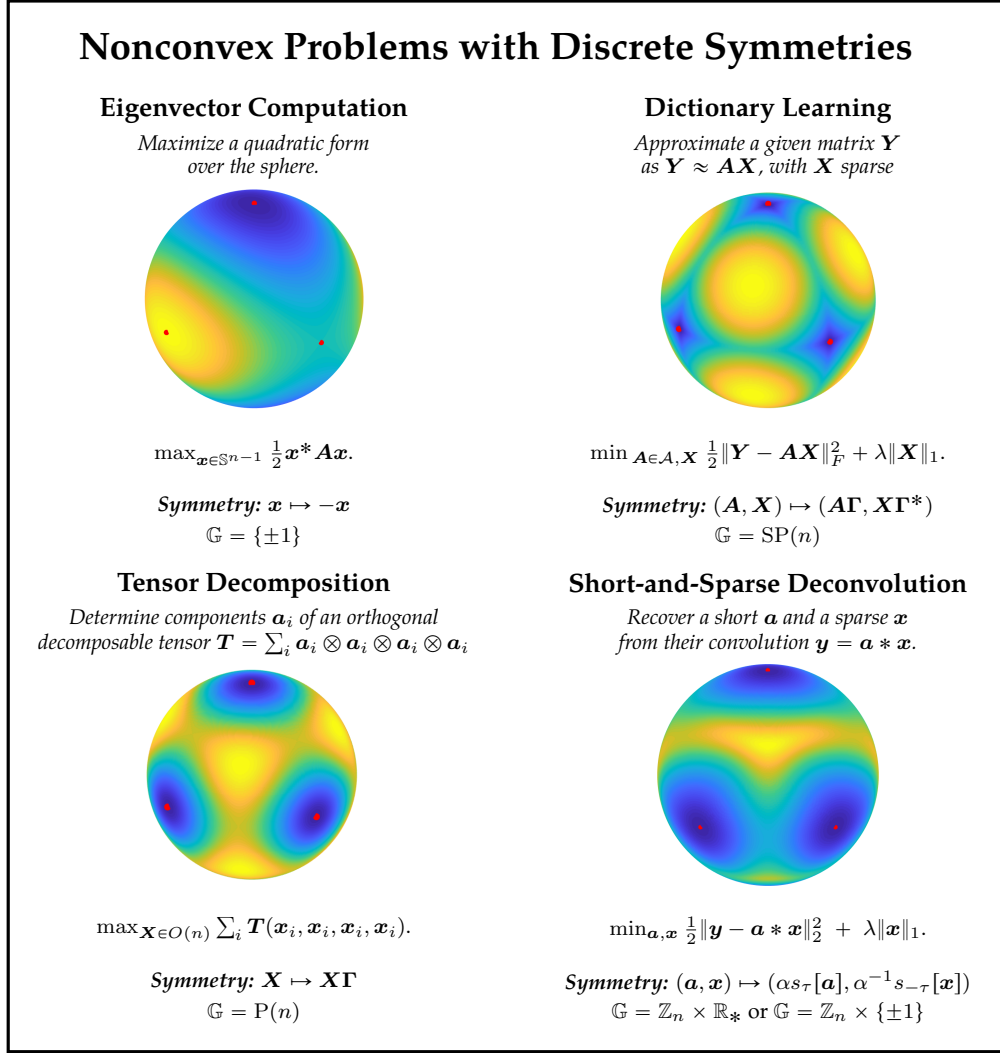


Figure 5: Four examples of problems with discrete symmetries. We discuss this family of problems in more detail in Section 3.

2 Nonconvex Problems with Rotational Symmetry

In this section, we study the first main class of problems in our taxonomy of symmetric nonconvex problems: problems with rotational symmetry. This class includes important model problems in phase recovery [3, 49] and low-rank estimation [11]. We begin by developing a few basic intuitions through a toy phase retrieval problem; we then show how these intuitions help to explain the geometry of a range of problems from imaging and machine learning.

2.1 One Minimal Example: Phase Retrieval with a Single Unknown

We first consider a model problem, in which our goal is to recover a single complex scalar $x_0 \in \mathbb{C}$ from m magnitude measurements

$$y_1 = |a_1 x_0|, \dots, y_m = |a_m x_0|, \quad (2.1)$$

where $a_1, \dots, a_m \in \mathbb{C}$ are known complex scalars. Collecting our observations y_i into a single vector $\mathbf{y} \in \mathbb{R}^m$ and collecting the a_i into a single vector $\mathbf{a} \in \mathbb{C}^m$, we can express this measurement model more compactly as

$$\mathbf{y} = |\mathbf{a} x_0|. \quad (2.2)$$

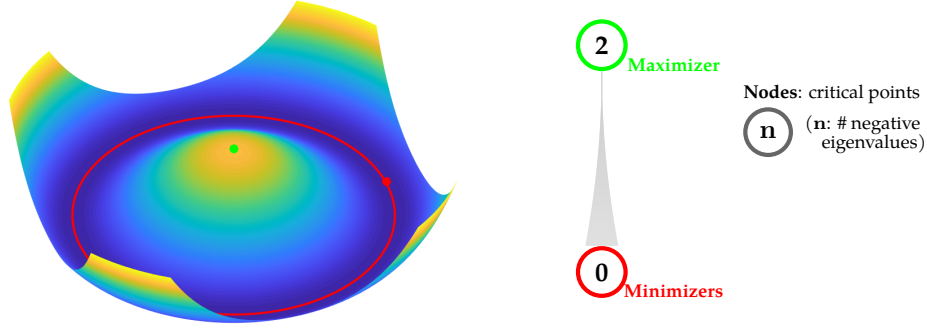


Figure 6: Phase Retrieval with a Single Unknown. We plot the objective function $\varphi(x)$ for phase retrieval with a single complex unknown. All **local minimizers** (red) are symmetric copies $x_0 e^{i\phi}$ of the ground truth $x_0 \in \mathbb{C}$. There is also a **local maximizer** (green) at $x = 0$; at this point, φ exhibits negative curvature in directions that break symmetry. Right: critical points arranged according to objective function φ , labelled according to their index (number of negative eigenvalues).

Our goal is to determine x_0 , up to a phase. This is a heavily simplified (indeed, trivialized!) version of the *generalized phase retrieval* problem [47, 48, 68], which we will describe in more detail in Section 2.2. Here our goal is simply to understand the consequences of the phase symmetry of the measurement model (2.2) for optimization. To this end, we study a model optimization problem,

$$\min_{x \in \mathbb{R}} \varphi(x) \doteq \frac{1}{2} \|\mathbf{y}^2 - |\mathbf{a}x|^2\|_2^2, \quad (2.3)$$

which minimizes the sum of squared differences between the squared magnitudes of $\mathbf{a}x$ and those of $\mathbf{a}x_0$. Note that

$$\varphi(x) = \frac{1}{4} \|\mathbf{a}\|_4^4 (|x|^2 - |x_0|^2)^2. \quad (2.4)$$

This is a function of a complex scalar $x = x_r + ix_i$. We can study its geometry by identifying x with a two-dimensional real vector $\bar{x} = (x_r, x_i)$. The slope and curvature of the function $\varphi(\bar{x})$ are captured by the gradient and Hessian,

$$\nabla \varphi(\bar{x}) = \|\mathbf{a}\|_4^4 \left(|x|^2 - |x_0|^2 \right) \begin{bmatrix} x_r \\ x_i \end{bmatrix}, \quad (2.5)$$

$$\nabla^2 \varphi(\bar{x}) = \|\mathbf{a}\|_4^4 \left((|x|^2 - |x_0|^2) \mathbf{I} + 2\bar{x}\bar{x}^* \right). \quad (2.6)$$

Figure 6 visualizes the objective $\varphi(\cdot)$ and its critical points. By setting $\nabla \varphi = 0$, and inspecting the Hessian, we obtain that there exist two families of critical points: global minimizers at $x = x_0 e^{i\phi}$, and a global maximizer at $x = 0$. We notice that:

- **Symmetric copies of the ground truth are minimizers.** The points $\{x_0 e^{i\phi}\}$ are the only local minimizers. In problems with phase ambiguities, we expect a circle $O(2) \cong \mathbb{S}^1$ of minimizers. In addition, the Hessian is positive semidefinite, but rank deficient at the global minimizers: the zero curvature direction (along which the objective φ is flat) is precisely the direction that is tangent to the set of equivalent solutions $g \cdot x_*$ at x_* . Normal to this set, the objective function exhibits positive curvature – a form of restricted strong convexity.
- **Negative curvature in symmetry breaking directions.** There is a local maximizer at $x = 0$, which is equidistant from the target solutions $\{x_0 e^{i\phi}\}$. At this point $\nabla^2 \varphi < \mathbf{0}$; there is negative curvature in every direction, and movement in any direction breaks the symmetry.

2.2 Generalized Phase Retrieval

The univariate phase retrieval problem is an extreme idealization of a basic problem in imaging: recovering a signal from phaseless measurements [3, 46]. This problem arises in many application areas, including electron

microscopy [69], diffraction and array imaging [70, 71], acoustics [72, 73], quantum mechanics [74, 75] and quantum information [76], where the goal is to image complex molecular structures. Illuminating a sample with coherent light produces a diffraction pattern, which is approximately the Fourier transform of the sample’s density. If we could measure this diffraction pattern, we could recover an image of the sample with atomic resolution, simply by inverting the Fourier transform. However, there is a wrinkle: typically, the magnitude of the Fourier transform is much easier to measure than the phase – the magnitude can be measured by aggregating energy over time, whereas measuring the phase of a high frequency signal requires the detector to be sensitive to very rapid changes. The Fourier phase retrieval problem asks us to reconstruct a complex signal from magnitude measurements only:

$$\text{find } \mathbf{x} \text{ such that } |\mathcal{F}[\mathbf{x}]| = \mathbf{y}.$$

This problem is widespread in scientific imaging [77–80], but it is quite challenging: it is ill-posed in one dimension, and in higher dimensions even the most effective numerical methods remain sensitive to initialization and parameter tuning [81], where for more details we refer readers to recent survey papers [3, 49, 82]. From the perspective of this survey, one explanation for this difficulty resides in the symmetries of the measurement operator $|\mathcal{F}[\cdot]|$: in addition to phase symmetry, the mapping $\mathbf{x} \mapsto |\mathcal{F}[\mathbf{x}]|$ is invariant under shifts and conjugate reversal of the signal \mathbf{x} .

In recent years, the applied mathematics community has investigated variants of the above problem in which the Fourier transform $\mathcal{F}(\cdot)$ is replaced by a more general linear operator $\mathcal{A}(\cdot)$ [46, 68, 83]. A “generic” map $\mathbf{x} \mapsto |\mathcal{A}[\mathbf{x}]|$ has simpler symmetries – typically only a phase symmetry, $|\mathcal{A}[\mathbf{x}e^{j\phi}]| = |\mathcal{A}[\mathbf{x}]|$. This makes generic phase recovery problems easier to study and easier to solve. While the Fourier model is more widely applicable to physical imaging, the generic phase retrieval model does capture aspects of certain less conventional imaging setups, including ptychography [84–86] (i.e., $\mathcal{A}(\cdot)$ is the Short Time Fourier Transform), coded illuminations [87, 88], and coded diffraction patterns [47]. A model one-dimensional⁷ version of the generalized phase retrieval problem can be formulated as follows:

$$\text{find } \mathbf{x} \in \mathbb{C}^n \text{ such that } |\mathbf{A}\mathbf{x}| = \mathbf{y}, \quad (2.7)$$

where $\mathbf{A} \in \mathbb{C}^{m \times n}$ is a matrix which represents the sensing process.

Analogous to the univariate phase retrieval in (2.3), we can attempt to recover \mathbf{x}_0 by minimizing its misfit to the observed data \mathbf{y} , by solving

$$\min_{\mathbf{x} \in \mathbb{C}^n} \varphi(\mathbf{x}) \equiv \frac{1}{4m} \sum_{k=1}^m \left(y_k^2 - |\mathbf{a}_k^* \mathbf{x}|^2 \right)^2, \quad (2.8)$$

where $\mathbf{a}_1, \dots, \mathbf{a}_m \in \mathbb{C}^n$ are the row vectors of \mathbf{A} . We saw from above that the univariate version of this function has a very simple landscape, which is dictated almost entirely by phase symmetry, and that it has no spurious local minimizers. *Should we expect similar behavior in this higher dimensional setting?*

Geometry of Generalized Phase Retrieval

One way of generating intuition is to assume that the sampling vectors $\{\mathbf{a}_i\}_{i=1}^m$ are chosen at random, and analyze $\varphi(\mathbf{x})$ using tools from statistics. Figure 7 visualizes $\varphi(\mathbf{x})$ when the \mathbf{a}_k are Gaussian vectors⁸ and m is large. As $m \rightarrow \infty$, $\varphi(\mathbf{x})$ converges to its expectation $\mathbb{E}_{\mathbf{a}}[\varphi]$, which can be calculated in closed form. In Figure 7 (left), we can see the characteristic phase symmetry, identical to our univariate example above. However, this problem is higher dimensional. Figure 7 (center) plots the objective over a two-dimensional slice containing the ground truth and an orthogonal direction, where we observe:

- **Symmetric copies of the ground truth are minimizers.** All the local minimizers are on the circle of points $\{\mathbf{x}_0 e^{i\phi}\}$, which corresponds to the ground truth up to the (rotational) phase symmetry. Problems with higher dimensional symmetries have larger sets of minimizers – e.g., $O(r)$ symmetry leads to a manifold of minimizers that is isometric to $O(r)$.

⁷Here, in comparison to the univariate case, one-dimensional means $\mathbf{x} \in \mathbb{C}^n$ is a vector instead of a matrix.

⁸Formally, \mathbf{a}_k are independent random vectors, with $\mathbf{a}_k = \mathbf{a}_k^r + i\mathbf{a}_k^i$ with \mathbf{a}_k^r and \mathbf{a}_k^i independent iid $\mathcal{N}(0, \frac{1}{2})$.

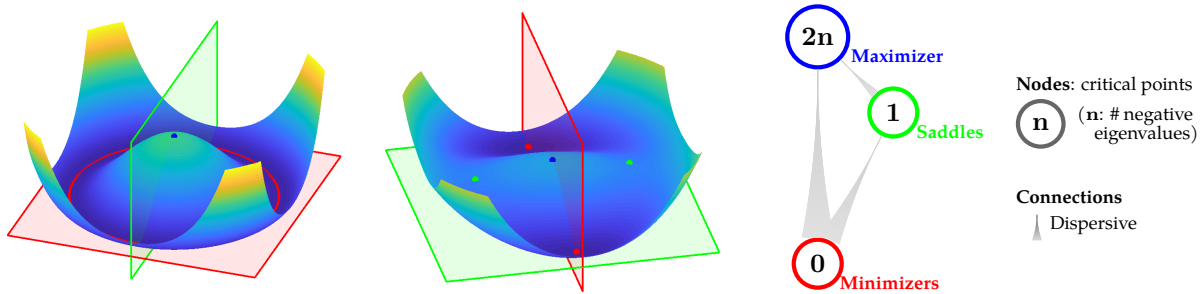


Figure 7: Generalized Phase Retrieval. We plot two slices of the landscape of the generalized phase retrieval problem with Gaussian measurements. Left: slice containing symmetric copies of the ground truth $x_0 e^{i\phi}$. Middle slice containing **minimizers** $x_0, -x_0$ and one orthogonal direction. Notice that at both the **maximizer** and **saddle points**, there is negative curvature in the direction that breaks symmetry between x_0 and $-x_0$. Right: critical points arranged according to objective $\mathbb{E}\varphi$, labeled with their indices (number of negative eigenvalues). Connections between critical points are “dispersive”: downstream negative curvature directions are the image of upstream negative curvature directions under gradient flow (see Appendix B).

- **Negative curvatures in symmetry-breaking directions.** In higher dimensional examples, we encounter a variety of local maximizers, saddle points, etc. Nevertheless, these critical points occur near balanced superpositions of equivalent solutions, and exhibit a negative curvature in directions $\pm x_0$, which breaks the symmetry.
- **Cascade of saddle points.** As shown schematically in Figure 7, the critical points can be graded based on the number of negative eigenvalues of the Hessian: critical points with higher objective values have more negative eigenvalues. Moreover, the objective has a “dispersive” property: upstream negative curvature discourages stagnation near the stable manifold of downstream critical points (see Appendix B for more detail).

Finite Samples, Structured Measurements, Different Objectives

The exposition in the previous section is still quite idealized: the measurements are Gaussian, and we have infinitely many of them. Moreover, we have assumed a particular objective $\varphi(x)$, which is not the common objective used in practice. Fortunately, the qualitative conclusions of the previous subsection carry over to more structured and challenging settings for generalized phase retrieval.⁹ In the following, we briefly describe these extensions, while noting technical caveats and open problems.

Finite Samples Phase retrieval is a sensing problem; measurements cost resources. It is important to minimize the number of measurements m required to accurately reconstruct x . Under the Gaussian model, the particular loss function $\varphi(\cdot)$ in (2.8) is a sum of independent heavy-tailed random variables. Relatively straightforward considerations show that when $m \gtrsim n^2$, gradients and Hessians concentrate uniformly about their expectations, and the objective has no spurious local minimizers. This number of samples is clearly suboptimal – n^2 measurements to recover about n complex numbers. The challenge is that the objective function (2.8) contains fourth moments of Gaussian variables, and its distribution is therefore heavy-tailed. Using arguments that are tailored to this situation, the required number of samples can be improved to $m \gtrsim n \log^3 n$ [48]. Moreover, modifying the objective (2.8) to remove large terms (ala robust statistics) can improve this to essentially optimal ($m \gtrsim n$) [89].¹⁰

⁹But *not* to the Fourier model, which has different symmetries. We discuss challenges and open problems around Fourier measurements in Section 3 and Section 4.

¹⁰Other approaches to producing analyses with small sample complexity include restricting the analysis to a small neighborhood of the ground truth, and initializing in this neighborhood using spectral methods that leverage the statistics of the measurement model [47, 90], or forgoing uniform geometric analysis and directly reasoning about trajectories of randomly initialized gradient descent [91].

Different Objective Functions The “squares of the squares” formulation in (2.8) is smooth and hence simple to analyze, but is typically not preferred in practice, especially when observations are noisy. Alternatives include $\varphi(\mathbf{x}) = \sum_i |y_i^2 - |\mathbf{a}_i^* \mathbf{x}|^2|$ [92, 93], $\varphi(\mathbf{x}) = \sum_i |y_i - |\mathbf{a}_i^* \mathbf{x}||^2$ [94], and maximum likelihood formulations that model (Poisson) noise in the observations y_i [89, 95]. Although these formulations differ in details, the major features of the objective landscape are independent of the choice of φ . For Gaussian sensing vectors $\{\mathbf{a}_i\}_{i=1}^m$, the expectation $\mathbb{E}_{\mathbf{a}} \{\varphi\}$ has no spurious minimizers; moreover, all objectives have a minimizer at zero and a family of saddle points orthogonal to \mathbf{x}_0 . However, proving (or disproving) that these objectives have benign global geometry for finite m is still an open problem. Existing small sample analyses [89, 92, 94] control the behavior of the objective in a neighborhood of $\mathbf{x}_0 e^{i\phi}$, and initialize in this neighborhood using statistical properties of the measurement model.

Structured Measurements Geometric intuitions for Gaussian \mathbf{A} carry over to several models that are more closely connected with imaging practice. Examples include convolutional models, in which we observe the modulus of the convolution $\mathbf{y} = |\mathbf{a} * \mathbf{x}|$ of the unknown signal \mathbf{x} with a known sequence \mathbf{a} [96] and coded diffraction patterns, in which we make multiple observations $\mathbf{y}_l = |\mathcal{F}[\mathbf{d}_l \circ \mathbf{x}]|$, where \circ denotes an elementwise product [83]. If the filter \mathbf{a} or the masks \mathbf{d}_l are chosen at random from appropriate distributions, these structured measurements yield the same asymptotic objective function $\mathbb{E}\varphi$. In particular, in the large sample limit (i.e., infinite long filter \mathbf{a} for the convolutional model, or infinitely many diffraction patterns \mathbf{d}_l in the coded diffraction model), these measurements still lead to optimization problems with no spurious local minimizers. Similar to the situation with nonsmooth objective functions, the best known theoretical sample complexities are obtained by initializing near the ground truth, using statistical properties of \mathbf{A} . Globally analyzing structured measurements in the small sample regime is a challenging open problem.

The above discussion only scratches the surface of the growing literature on generalized phase retrieval, we refer readers to [3, 49, 82, 97] for a more comprehensive survey on recent developments. From the perspective of this survey, the unifying thread through all of these models, objectives and problems is the simple model geometry in Figure 7. In the next section, we will see a similar phenomenon with low-rank matrices: a model geometry originating in matrix factorization recurs across a sequence of increasingly challenging matrix recovery problems.

2.3 Low Rank Matrix Recovery

The problem of recovering a low-rank matrix from incomplete and unreliable observations finds broad applications in robust statistics, recommender systems, data compression, computer vision, and so on [98]. In matrix recovery problems, the goal is to estimate a matrix $\mathbf{X}_0 \in \mathbb{R}^{n_1 \times n_2}$ from incomplete or noisy observations. Typically, this problem is ill-posed without any assumptions on the matrix \mathbf{X}_0 . In many applications where the data are highly structured, \mathbf{X}_0 can be assumed to be *low rank*, or approximately so:

$$r = \text{rank}(\mathbf{X}_0) \ll \min\{n_1, n_2\}. \quad (2.9)$$

Additionally, any rank- r matrix can be expressed as a product of a tall $n_1 \times r$ matrix and a wide $r \times n_2$ matrix:

$$\mathbf{X}_0 = \mathbf{U}\mathbf{V}^*, \quad \mathbf{U} \in \mathbb{R}^{n_1 \times r}, \mathbf{V} \in \mathbb{R}^{n_2 \times r}. \quad (2.10)$$

A very popular strategy for recovering \mathbf{X}_0 is to start with some objective function $\psi(\mathbf{X})$ that enforces consistency with observed data, and then parameterize \mathbf{X} in terms of the factors \mathbf{U}, \mathbf{V} [99], yielding the optimization problem

$$\min_{\mathbf{U}, \mathbf{V}} \varphi(\mathbf{U}, \mathbf{V}) \equiv \psi(\mathbf{U}\mathbf{V}^*), \quad (2.11)$$

where we shall discuss the concrete form of the loss $\varphi(\cdot)$ later in this section (i.e., see (2.16)).

Symmetries of Low Rank Models

Formulations like (2.11) are almost always nonconvex in the factors \mathbf{U} and \mathbf{V} , due to symmetries of the factorization (2.10). Indeed, for any invertible matrix $\mathbf{\Gamma} \in \mathbb{R}^{r \times r}$,

$$\mathbf{U}\mathbf{V}^* = \mathbf{U}\mathbf{\Gamma}\mathbf{\Gamma}^{-1}\mathbf{V}^* = (\mathbf{U}\mathbf{\Gamma})(\mathbf{V}\mathbf{\Gamma}^{-*})^* \quad (2.12)$$

Because of this ambiguity, the problem (2.11) always possess a *general linear* (invertible matrix) symmetry:

$$(\mathbf{U}, \mathbf{V}) \equiv (\mathbf{U}\mathbf{\Gamma}, \mathbf{V}\mathbf{\Gamma}^{-*}), \quad \mathbf{\Gamma} \in \text{GL}(r). \quad (2.13)$$

As the determinant of a general linear matrix $\mathbf{\Gamma}$ can be arbitrarily close to zero, and hence be arbitrarily ill-conditioned, the equivalence class of solutions (\mathbf{U}, \mathbf{V}) has somewhat complicated geometry, as a subset of $\mathbb{R}^{n_1 \times r} \times \mathbb{R}^{n_2 \times r}$.¹¹ Fortunately, as we shall see in the following, it is not difficult to reduce this general linear symmetry to a simpler and better conditioned orthogonal symmetry, either by using information about the target \mathbf{X}_0 , or by adding additional regularization terms to (2.11).

Rotational Symmetries for Symmetric \mathbf{X}_0 If we have extra information that the target solution \mathbf{X}_0 is *symmetric and positive semidefinite*, then it admits a factorization of the form $\mathbf{X}_0 = \mathbf{U}_0\mathbf{U}_0^*$. Thus, we can take $\mathbf{U} = \mathbf{V}$, which gives a slightly simpler problem

$$\min_{\mathbf{U}} \varphi(\mathbf{U}) \equiv \psi(\mathbf{U}\mathbf{U}^*), \quad (2.14)$$

with a smaller symmetry group. For any $\mathbf{\Gamma} \in O(r)$, $\mathbf{U}\mathbf{U}^* = \mathbf{U}\mathbf{\Gamma}\mathbf{\Gamma}^*\mathbf{U}^* = (\mathbf{U}\mathbf{\Gamma})(\mathbf{U}\mathbf{\Gamma})^*$, and so the symmetric problem (2.14) exhibits an orthogonal/rotational symmetry that $\mathbf{U} \equiv \mathbf{U}\mathbf{\Gamma}$, for $\mathbf{\Gamma} \in O(r)$.

Rotational Symmetries for General \mathbf{X}_0 via Penalization For general (non-symmetric) matrices \mathbf{X} , it is possible to add additional regularizations to (2.11) in such a way that the general linear symmetry reduces to an orthogonal symmetry. At a high level, the idea is to add a penalty $\rho(\mathbf{U}, \mathbf{V})$ that enforces $\mathbf{U}^*\mathbf{U} \approx \mathbf{V}^*\mathbf{V}$; this prevents \mathbf{U} and \mathbf{V} from having vastly imbalanced scales.¹² The penalty ρ can be chosen such to be $O(r)$ -symmetric, such that the combined problem

$$\min_{\mathbf{U}, \mathbf{V}} \varphi(\mathbf{U}, \mathbf{V}) + \rho(\mathbf{U}, \mathbf{V}), \quad (2.15)$$

possesses a simple $O(r)$ symmetry: $(\mathbf{U}, \mathbf{V}) \equiv (\mathbf{U}\mathbf{\Gamma}, \mathbf{V}\mathbf{\Gamma})$, for $\mathbf{\Gamma} \in O(r)$.

Model Problems and the Matrix Recovery Zoo. There are many variants of the vanilla matrix recovery problem, which are motivated by different applications and impose different assumptions on the observations and the noise [11, 51, 98]. Although these problems have their own technical challenges, they have certain qualitative features in common. At a high level, “matrix *recovery* problems act like matrix *factorization* problems” [51]. In the next section, we will begin by describing in detail the geometry of matrix factorization, and then describe how these intuitions carry over to matrix recovery from incomplete or unreliable observations.

Geometry of Matrix Factorization

Our first model problem starts with a complete, noise-free observation $\mathbf{Y} = \mathbf{X}_0$ of a symmetric, positive semidefinite matrix $\mathbf{X}_0 \in \mathbb{R}^{n \times n}$ of rank $r < n$, and attempts to factor it as $\mathbf{X}_0 = \mathbf{U}\mathbf{U}^*$ by minimizing the misfit to the observed data [100]:

$$\min_{\mathbf{U} \in \mathbb{R}^{n \times r}} \varphi(\mathbf{U}, \mathbf{U}) \doteq \frac{1}{4} \|\mathbf{Y} - \mathbf{U}\mathbf{U}^*\|_F^2. \quad (2.16)$$

This is a nonconvex optimization problem, with orthogonal symmetry $\mathbf{U} \equiv \mathbf{U}\mathbf{\Gamma}$. Figure 8 visualizes the objective landscape for this problem. It turns out that the critical points of φ are dictated by the eigen-decomposition of the symmetric matrix \mathbf{X}_0 – *every critical point \mathbf{U} is generated by selecting and appropriately scaling a subset of the eigenvectors of \mathbf{X}_0 , and then applying a right rotation $\mathbf{U} \mapsto \mathbf{U}\mathbf{R}$* . At a slogan level, critical points correspond to “under-factorizations” of the ground truth. By inspecting the hessian, we find that:

- **Symmetric copies of the ground truth are minimizers.** Local minimizers are the critical points which select all of the top r eigenvectors, which correspond to the ground truth up to a rotation symmetry;

¹¹For example, it is neither closed nor bounded.

¹²For example, $\rho(\mathbf{U}, \mathbf{V}) = \frac{1}{2} \|\mathbf{U}^*\mathbf{U} - \mathbf{V}^*\mathbf{V}\|_F$ accomplishes this.

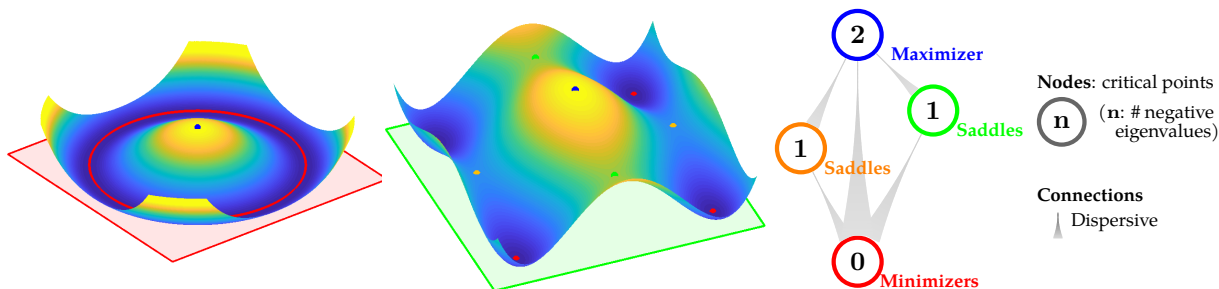


Figure 8: Geometry of Matrix Factorization. Geometry of a model problem in which the target \mathbf{X}_0 is a symmetric matrix of rank two, with eigenvalues $\frac{3}{4}$ and $\frac{1}{2}$. Left: plot of the objective φ over a slice of the domain containing all optimal solutions. Center: two families of saddle points, corresponding to rank-one approximations. Right: objective value φ versus index for the four families of critical points in this problem. Again the critical points are *graded*, in the sense that φ decreases with decreasing index, and the paths between them are dispersive, in the sense that downstream negative curvature directions are the image of upstream negative curvature directions under gradient flow.

- *Negative curvature in symmetry-breaking directions.* At a saddle point, there are strict negative curvatures in any directions which increase the number of top eigenvectors that participate.
- *Cascade of saddle points.* Saddle points are critical points selecting subsets of the top r eigenvectors. These saddle points can be graded based on the number of selected eigenvectors.¹³

Figure 8 (center) visualizes these effects. This model geometry carries over to non-symmetric matrices. For example, considering a penalized low-rank estimation problem

$$\min_{U \in \mathbb{R}^{n_1 \times r}, V \in \mathbb{R}^{n_2 \times r}} \varphi(U, V) \doteq \frac{1}{4} \|\mathbf{Y} - UV^*\|_F^2 + \rho(U, V), \quad (2.17)$$

we obtain a problem with $O(r)$ symmetry. Critical points are generated by appropriately scaling subsets of the *singular* vectors of \mathbf{Y} – see Appendix A for details on both of these geometries.

From Matrix Factorization to Matrix Recovery and Completion

We next describe how precise geometric analyses of matrix factorization extend to a more realistic problem of recovering a low-rank matrix from incomplete and unreliable observations. As we shall see, matrix recovery problems often retain important qualitative features of matrix factorization. We will illustrate this phenomenon through several instances of a model recovery problem, in which we observe m linear functions of an unknown matrix $\mathbf{X}_0 \in \mathbb{R}^{n_1 \times n_2}$:

$$y_i = \langle \mathbf{A}_i, \mathbf{X}_0 \rangle, \quad 1 \leq i \leq m, \quad (2.18)$$

and the goal is to recover \mathbf{X}_0 . This model is flexible enough to represent matrix completion from missing entries [101], as well as more exotic sensing problems [98, 102]. We can write this observation model more compactly by defining a linear operator $\mathcal{A} : \mathbb{R}^{n_1 \times n_2} \rightarrow \mathbb{R}^m$ with $\mathcal{A}(\mathbf{X}) := [\langle \mathbf{A}_i, \mathbf{X} \rangle]_{1 \leq i \leq m}$. In this notation,

$$\mathbf{y} = \mathcal{A}(\mathbf{X}). \quad (2.19)$$

If $m < n_1 n_2$, the number of observations is smaller than the number of unknowns, and the recovery problem is ill-posed. Fortunately, matrices encountered in applications have low-complexity structures; for instance, they are usually low-rank or approximately so. As above, a rank- r matrix \mathbf{X}_0 admits a factorization $\mathbf{X}_0 = \mathbf{U}_0 \mathbf{V}_0^*$,

¹³A natural descent algorithm only visit at most r saddle points whose trajectory depends on the containment of the active eigenvectors at those saddle points.

that we can enforce this low-rank structure by directly recovering the factors \mathbf{U} and \mathbf{V} , up to a rotational symmetry. A natural approach is to minimize the misfit to the observed data:

$$\min_{\mathbf{U}, \mathbf{V}} \varphi(\mathbf{U}, \mathbf{V}) \doteq \frac{1}{4m} \sum_{i=1}^m (y_i - \langle \mathbf{A}_i, \mathbf{U}\mathbf{V}^* \rangle)^2 + \rho(\mathbf{U}, \mathbf{V}) = \frac{1}{4m} \|\mathbf{y} - \mathcal{A}(\mathbf{U}\mathbf{V}^*)\|_2^2 + \rho(\mathbf{U}, \mathbf{V}), \quad (2.20)$$

where as above ρ is a regularizer that encourages the factors to be balanced.

Matrix Sensing If $\mathcal{A} = \mathcal{I}$ is an identity operator, then (2.20) simply reduces to the factorization problem. In this special situation, the measurement operator \mathcal{A} *exactly* preserves the geometry of *all* $n_1 \times n_2$ matrices, in the sense that $\|\mathcal{A}[\mathbf{X}]\|_2 = \|\mathbf{X}\|_F$ for all \mathbf{X} . However, when \mathcal{A} is a generic operator rather than an identity map, and the number of measurements is small ($m < n_1 n_2$), the exact geometric preservation becomes impossible. Fortunately, as long as \mathcal{A} *approximately* preserves the geometry of the *low-rank* matrices – a much lower dimensional set [100, 103–106], then (2.20) still “behaves like the factorization problem”, and hence can be used to recover \mathbf{X}_0 .¹⁴ When this approximation is sufficiently accurate, there is a bijection between the critical points of the sensing problem (2.20) and those of factorization, which preserves the index (number of negative eigenvalues). Under this condition, every local minimum of the sensing problem is global [104].

Matrix Completion The most practical and important instance of the general sensing model (2.20) is the *matrix completion* problem [101], in which the goal is to recover a low-rank matrix from a subset of its entries. This model problem arises, e.g., in collaborative filtering [107, 108], where the goal is to predict users’ preferences for various products based a few observed preferences. Variants of this problem also appear in sensor networks (determining positions of sensors from a few distance measurements) [109, 110], imaging (recovering shape from illumination) [111, 112] and the geosciences [113, 114], just to name a few.

Matrix completion also inherits the geometry of matrix factorization, with several technical caveats, which are consequences of the fact that it is challenging to recover \mathbf{X}_0 whose energy is concentrated on a small number of entries: if we fail to sample these important entries, we will fail to recover \mathbf{X}_0 . This basic issue affects both for the well-posedness of the matrix completion problem and for our ability to solve it globally using nonconvex optimization. Local optimization methods could potentially become trapped in the region of the space in which $\mathbf{U}\mathbf{V}^*$ is nearly sparse, since the measurements do not effectively sense such matrices. One simple fix is to add an additional regularizer on the rows \mathbf{u}_i and \mathbf{v}_i of the factors, which encourages them to have small norm. This forces the energy of $\mathbf{U}\mathbf{V}^*$ to be spread across many entries.¹⁵ In particular, Ge et al. [50] proved that the resulting problem has a benign global geometry whenever we observe a sufficiently large random subset Ω and the target matrix \mathbf{X}_0 is itself not too concentrated on a few entries, in a precise technical sense.¹⁶

Robust Matrix Recovery Many data analysis problems confront the analyst with data sets that are not only incomplete, but also corrupted. Robust matrix recovery is the problem of estimating a low-rank matrix \mathbf{X}_0 from such an unreliable observation. Different models of corruption may be applicable in different application scenarios. For example, in imaging and vision, individual features (entries of the matrix) may be corrupted, e.g., due to occlusion [115, 116]. This can be modeled as a sparse error: $\mathbf{Y} = \mathbf{X}_0 + \mathbf{S}_0$, with both $\mathbf{X}_0 = \mathbf{U}_0 \mathbf{V}_0^*$ and \mathbf{S}_0 unknown. We start from a natural formulation

$$\min_{\mathbf{U}, \mathbf{V}, \mathbf{S}} \frac{1}{2} \|\mathbf{U}\mathbf{V}^* + \mathbf{S} - \mathbf{Y}\|_F^2 + g_s(\mathbf{S}) + \rho_r(\mathbf{U}, \mathbf{V}), \quad (2.21)$$

where $g_s(\mathbf{S})$ is a regularizer that encourages \mathbf{S} to be sparse. Partially minimizing with respect to \mathbf{S} , we obtain

$$\min_{\mathbf{U}, \mathbf{V}} \psi(\mathbf{U}\mathbf{V}^* - \mathbf{Y}) + \rho_r(\mathbf{U}, \mathbf{V}), \quad (2.22)$$

where $\psi(\cdot)$ is a new function that measures data fidelity – e.g., if g_s is the ℓ^1 norm, then ψ is a *Huber function* [117]. This is again a matrix factorization problem, but with a different loss $\psi(\mathbf{U}\mathbf{V}^* - \mathbf{Y})$. While there are

¹⁴This intuition can be formalized through the *rank restricted isometry property* (rank RIP) [98, 102].

¹⁵In details, one can add a penalty $\rho_{\text{mc}}(\mathbf{U}, \mathbf{V}) = \lambda_1 \sum_{i=1}^{n_1} (\|\mathbf{e}_i^* \mathbf{U}\|_2 - \alpha_1)_+^4 + \lambda_2 \sum_{j=1}^{n_2} (\|\mathbf{e}_j^* \mathbf{V}\|_2 - \alpha_2)_+^4$ to (2.20)

¹⁶Formally, \mathbf{X}_0 is μ -incoherent, in the sense that for its compact SVD $\mathbf{X}_0 = \mathbf{B}\mathbf{\Sigma}\mathbf{C}^*$, $\|\mathbf{e}_i^* \mathbf{B}\|_2 \leq \sqrt{\mu r/n_1}$ and $\|\mathbf{e}_j^* \mathbf{C}\|_2 \leq \sqrt{\mu r/n_2}$.

a number of open issues around the global (and even local! [118, 119]) geometry of this problem, known results again suggest that for certain choices of g_s and ρ_r it indeed inherits the geometry of factorization [11]. Similar to matrix completion, technical issues arise due to the possibility of encountering low-rank matrices UV^* that are themselves sparse. If the regularizer ρ_r is chosen to discourage such solutions, it is possible to prove that the resulting objective function has no spurious local minimizers, and negative curvature at every non-minimizing critical point.

Equation (2.21) is just one model for matrix recovery from unreliable observations. Versions in which entire columns of \mathbf{Y} are corrupted are also of interest for robust statistical estimation (see e.g., [120]), where they model outlying data vectors. Certain variants of this problem also inherit the geometry of factorization – local minimizers are global, saddle points are generated by partial factorizations of the ground truth, and exhibit negative curvature in directions that introduce additional ground truth factors [121–123]. It is also possible to formulate this version of the robust matrix recovery problem as one of finding a hyperplane that contains the majority of the datapoints. This dual viewpoint leads to nonconvex problems with a sign symmetry, which again have benign geometry under certain conditions on the input data [124–127].

3 Nonconvex Problems with Discrete Symmetry

In this section, we study nonconvex problems with discrete symmetry groups \mathbb{G} . Canonical examples include sparse dictionary learning (signed permutation symmetry) [20, 52, 53, 128], sparse blind deconvolution (signed shift symmetry) [55–59, 129], tensor decomposition [22, 60] and clustering (permutation symmetry). Unlike the problem we discussed in Section 2, the problems of this type are not easily amenable to convexification; understanding nonconvex optimization landscapes becomes more critical. Design choices, such as the choice of objective function and constraints, also seem to play a critical role: many of the examples we review below are formulated as constrained optimization problems over compact manifolds such as spheres or orthogonal groups. We again begin by studying a very simple model problem: dictionary learning with one-sparse data. We extract several key intuitions for problems with discrete symmetries, and then examine how these intuitions carry over to less idealized (and more useful!) problem settings.

3.1 Minimal Example: Dictionary Learning with One-Sparse Data

Similar to We introduce some basic intuitions through a model problem, which is a highly idealized version of *dictionary learning*. In this model problem, we observe a matrix \mathbf{Y} which is the product of an orthogonal matrix $\mathbf{A}_0 \in O(m)$ (called a dictionary) and a matrix $\mathbf{X}_0 \in \mathbb{R}^{m \times n}$ whose columns are one-sparse, i.e., each column of \mathbf{X}_0 has one nonzero entry:

$$\mathbf{Y} = \underbrace{\mathbf{A}_0}_{\text{orthogonal dictionary}} \underbrace{\mathbf{X}_0}_{\text{1-sparse coefficients}}. \quad (3.1)$$

This observation model exhibits a **signed permutation symmetry** ($\mathbb{G} = \text{SP}(n)$): for a given pair $(\mathbf{A}_0, \mathbf{X}_0)$, and any $\mathbf{\Gamma} \in \text{SP}(n)$, the pair $(\mathbf{A}_0\mathbf{\Gamma}, \mathbf{\Gamma}^*\mathbf{X}_0)$ also reproduces \mathbf{Y} . The goal is to recover \mathbf{A}_0 and \mathbf{X}_0 , up to this signed permutation symmetry. A natural approach for recovering \mathbf{A}_0 is to search for an orthogonal matrix \mathbf{A} such that $\mathbf{A}^*\mathbf{Y}$ is *as sparse as possible*:

$$\min h(\mathbf{A}^*\mathbf{Y}) \quad \text{s.t.} \quad \mathbf{A} \in O(m), \quad (3.2)$$

where $h(\mathbf{X}) = \sum_{ij} h(\mathbf{X}_{ij})$ encourages sparsity. There are many possible choices for h [128, 130, 131]; for concreteness, here we take h to be the Huber function [117] as

$$h_\lambda(u) = \begin{cases} \lambda|u| - \lambda^2/2 & |u| > \lambda, \\ u^2/2 & |u| \leq \lambda. \end{cases} \quad (3.3)$$

The Huber loss can be viewed as a differentiable surrogate for the (sparsity promoting) ℓ^1 norm.

In (3.2), finding the entire dictionary $\mathbf{A}_0 = [\mathbf{a}_{01}, \dots, \mathbf{a}_{0m}]$ at once could still be quite challenging. Instead, an even simpler model problem is to solve for one column \mathbf{a}_{0i} of \mathbf{A}_0 once at a time:

$$\min_{\mathbf{a}} h_\lambda(\mathbf{a}^*\mathbf{Y}) \quad \text{such that} \quad \mathbf{a} \in \mathbb{S}^{m-1}. \quad (3.4)$$

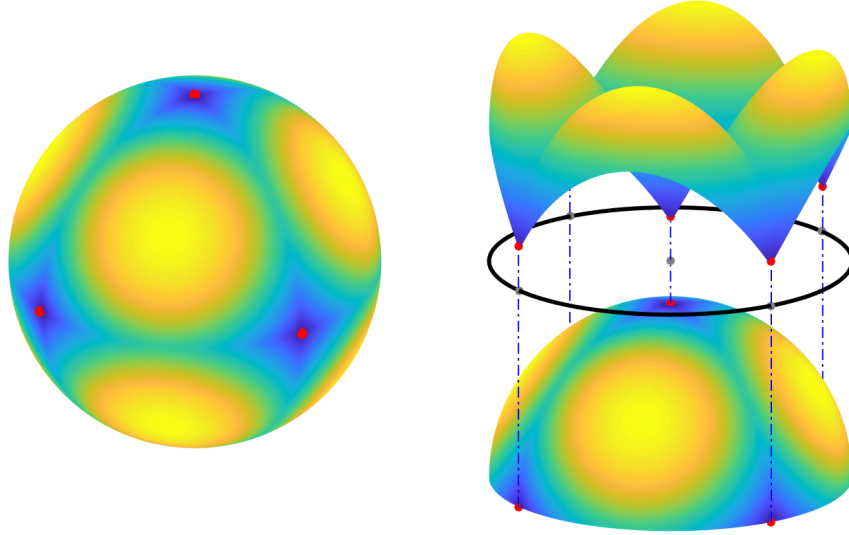


Figure 9: A model problem with discrete symmetry. Left: $h_\lambda(\mathbf{u})$ as a function on the sphere \mathbb{S}^2 . Local minimizers (red) are signed standard basis vectors $\pm \mathbf{e}_i$. These are the maximally sparse vectors on \mathbb{S}^2 . Right: graph of h_λ ; notice the strong negative curvature at points that are not sparse.

Here, our goal is to recover a signed column $\pm \mathbf{a}_{0i}$ of the dictionary \mathbf{A}_0 .¹⁷ This problem asks us to minimize an ℓ^1 -like function over the sphere.¹⁸

To further simplify matters, we assume that the true dictionary \mathbf{A}_0 is an identity matrix. This does not change our geometric conclusions – changing to another orthogonal \mathbf{A}_0 simply rotates the objective function. Similarly, because for this model problem each column of \mathbf{X}_0 has only one nonzero entry, we lose little generality in taking $\mathbf{X}_0 = \mathbf{I}$. With these idealizations, the problem simply becomes one of minimizing a sparsity surrogate over the sphere

$$\min \varphi(\mathbf{a}) \equiv h_\lambda(\mathbf{a}) \quad \text{such that} \quad \mathbf{a} \in \mathbb{S}^{m-1}. \quad (3.5)$$

Here, recovering a signed column of the true dictionary $\mathbf{A}_0 = \mathbf{I}$ corresponds to recovering one of the signed standard basis vectors $\pm \mathbf{e}_1, \dots, \pm \mathbf{e}_m$.

Geometry of the Model Problem The 1-sparse dictionary learning model problem also exhibits a signed permutation symmetry: for any $\Gamma \in \text{SP}(m)$, $\varphi(\Gamma \mathbf{a}) = \varphi(\mathbf{a})$. The set of target solutions $\pm \mathbf{e}_1, \dots, \pm \mathbf{e}_m$ is also symmetric. Figure 9 plots the objective function, and these target solutions, in a three dimensional example. Clearly, in this example, these target solutions are the only local minimizers.

To study this phenomenon more formally, we need to understand the slope (gradient) and curvature (Hessian) of φ as a function over the sphere \mathbb{S}^{m-1} . We develop these objects in an intuitive fashion. The sphere is a smooth manifold; its tangent space at a point \mathbf{a} can be identified with the set of vectors \mathbf{a}^\perp that are perpendicular to \mathbf{a} :

$$T_{\mathbf{a}} \mathbb{S}^{m-1} = \{ \boldsymbol{\delta} \mid \mathbf{a}^* \boldsymbol{\delta} = 0 \}.$$

The orthogonal projector onto the tangent space is simply given by $\mathbf{P}_{\mathbf{a}^\perp} = \mathbf{I} - \mathbf{a} \mathbf{a}^*$. The slope of φ over the sphere (formally, the Riemannian gradient) is simply the component of the standard gradient that is tangent to the sphere:

$$\text{grad}[\varphi](\mathbf{a}) = \mathbf{P}_{\mathbf{a}^\perp} \nabla \varphi(\mathbf{a}) \quad (3.6)$$

¹⁷The entire dictionary can be recovered by solving a sequence of problems of this type; see [20, 52, 132].

¹⁸The problem (3.4) can also be interpreted geometrically as searching for a sparse vector in the linear subspace $\text{row}(\mathbf{Y})$; see also [63, 133].

The curvature of φ over the sphere is slightly more complicated than that of the Euclidean case. For a direction $\delta \in T_{\mathbf{a}}\mathbb{S}^{m-1}$, the second derivative of φ along the geodesic curve (great circle) $\gamma(t) = \exp_{\mathbf{a}}(t\delta)$ is given by $\delta^* \text{Hess}[\varphi](\mathbf{a})\delta$, where $\text{Hess}[\varphi]$ denotes the *Riemannian Hessian*

$$\text{Hess}[\varphi](\mathbf{a}) = \mathbf{P}_{\mathbf{a}^\perp} \left(\begin{array}{c} \nabla^2 \varphi(\mathbf{a}) \\ \text{curvature of } \varphi \end{array} - \begin{array}{c} \langle \nabla \varphi(\mathbf{a}), \mathbf{a} \rangle \mathbf{I} \\ \text{curvature of the sphere} \end{array} \right) \mathbf{P}_{\mathbf{a}^\perp}. \quad (3.7)$$

This expression contains two terms. The first is the standard (Euclidean) Hessian $\nabla^2 \varphi$, which accounts for the curvature of the objective function φ . The second term accounts for the curvature of the sphere itself.¹⁹ Analogous to the case in the Euclidean space, critical points are characterized by Riemannian gradient $\text{grad}[\varphi](\mathbf{a}) = \mathbf{0}$; curvature can be studied through $\text{Hess}[\varphi](\mathbf{a})$. For more technical details, we refer readers to [134, 135].

To study the critical points, we begin by calculating the Euclidean gradient of φ :

$$\nabla \varphi(\mathbf{a}) = \lambda \text{sign}(\mathbf{a}) \odot \mathbb{1}_{|\mathbf{a}| > \lambda} + \mathbf{a} \odot \mathbb{1}_{|\mathbf{a}| \leq \lambda}, \quad (3.8)$$

where the Hadamard product \odot denotes elementwise multiplication. Using this expression, we can show that the Riemannian gradient vanishes ($\text{grad}[\varphi](\mathbf{a}) = \mathbf{0}$) if and only if $\nabla \varphi(\mathbf{a}) \propto \mathbf{a}$ (here, \propto denotes proportionality, i.e., $\exists s$ such that $\nabla \varphi(\mathbf{a}) = s\mathbf{a}$). This occurs whenever

$$\mathbf{a} \propto \text{sign}(\mathbf{a}). \quad (3.9)$$

We can therefore index critical points by the support I and sign pattern σ of \mathbf{a} , writing $\mathbf{a}_{I,\sigma}$. To understand which critical points are minimizers, we can study the Riemannian Hessian $\text{Hess}[\varphi](\mathbf{a})$. The Euclidean Hessian is $\nabla^2 \varphi(\mathbf{a}) = \mathbb{1}_{|\mathbf{a}| \leq \lambda}$; its Riemannian counterpart is

$$\text{Hess}[\varphi](\mathbf{a}_{I,\sigma}) = \mathbf{P}_{\mathbf{a}_{I,\sigma}^\perp} (\mathbf{P}_{|\mathbf{a}_{I,\sigma}| \leq \lambda} - \lambda |I| \mathbf{I}) \mathbf{P}_{\mathbf{a}_{I,\sigma}^\perp}. \quad (3.10)$$

At critical points $\mathbf{a}_{I,\sigma}$ the Hessian exhibits $(|I| - 1)$ negative eigenvalues, and $n - |I|$ positive eigenvalues. Based on these calculations, we draw the following conclusions on the geometry of φ :

- **Symmetric copies of the ground truth are minimizers.** Local minimizers are the signed standard basis vectors $\mathbf{a} = \pm \mathbf{e}_i$ with strictly positive Riemannian Hessians; the objective function is strongly convex in the vicinity of local minimizers.
- **Negative curvature in symmetry breaking directions.** Saddle points are balanced superpositions of target solutions: $\mathbf{a}_{I,\sigma} = \frac{1}{\sqrt{|I|}} \sum_{i \in I} \sigma_i \mathbf{e}_i$ for $I \subseteq \{1, \dots, m\}$ and signs $\sigma_i \in \{\pm 1\}$. There are negative curvatures in directions $\delta \in \text{span}(\{\mathbf{e}_i \mid i \in I\})$ that break the balance between target solutions.
- **Cascade of saddle points.** Saddle points are graded: points $\mathbf{a}_{I,\sigma}$ with larger objective value have more directions of negative curvature. Moreover, similar to the examples discussed in the last section, the objective function exhibits a “dispersive” structure: downstream negative curvature directions are the image of upstream negative curvature directions under gradient flow. This means that negative curvature upstream helps to prevent local methods from stagnating near downstream saddle points.

In the following subsections, we shall see how these basic phenomena recur in more practical nonconvex problems with discrete symmetries, including general dictionary learning (Section 3.2), blind deconvolution (Section 3.3), and others.

3.2 Dictionary Learning

The one-sparse dictionary learning problem is an extreme simplification of basic modern data processing problem: seeking a concise representation of data. As already precluded in Section 3.1, the goal of dictionary learning is to produce a sparse model for an observed dataset $\mathbf{Y} = [\mathbf{y}_1, \dots, \mathbf{y}_p] \in \mathbb{R}^{m \times p}$. Namely, we seek matrices $\mathbf{A}_0 \in \mathbb{R}^{m \times n}$ and $\mathbf{X}_0 \in \mathbb{R}^{n \times p}$ such that

$$\mathbf{Y} \approx \begin{array}{c} \mathbf{A}_0 \\ \text{dictionary} \end{array} \begin{array}{c} \mathbf{X}_0 \\ \text{sparse coefficients} \end{array} \quad (3.11)$$

¹⁹This expression can be derived in a simple way by letting $\|\delta\|_2 = 1$, and calculating $\frac{d^2}{dt^2} \Big|_{t=0} \varphi(\mathbf{a} \cos t + \delta \sin t)$.

with \mathbf{X}_0 being as *sparse* as possible. Sparsity is desirable for data compression, which facilitates tasks such as sensing, denoising, and superresolution, etc. [136, 137]

In the representation (3.11), the data points \mathbf{y}_j are approximated as superpositions $\mathbf{y}_j \approx \mathbf{A}_0 \mathbf{x}_{0j}$ of a few columns of the dictionary $\mathbf{A}_0 \in \mathbb{R}^{m \times n}$. Clearly, the size of the dictionary, n , has an impact on the accuracy, sparsity, and utility of this data representation. The appropriate dictionary size depends on application: for learning from a single image, a complete ($n = m$) dictionary may suffice, whereas for learning from a larger collection of images, an overcomplete ($n > m$) dictionary may be more appropriate [138–140]. Below, we discuss how our basic intuitions obtained from the orthogonal and one-sparse case in Section 3.1, can be carried over to each of these more realistic model problems.

Complete Dictionary Learning There are two basic issues in moving from the one-sparse dictionary learning problem to more general complete dictionary learning problems, in which $\mathbf{A}_0 \in \mathbb{R}^{m \times m}$ is some invertible matrix. First, the target dictionary \mathbf{A}_0 may not be orthogonal. Second, the columns of the coefficient matrix \mathbf{X}_0 are generally not one-sparse. For theoretical purposes, both of these issues can be addressed using probabilistic properties of \mathbf{X}_0 . First, using the statistics of $\mathbf{Y} = \mathbf{A}_0 \mathbf{X}_0$ it is possible to reduce the problem of learning a general invertible \mathbf{A}_0 to one of learning an orthogonal matrix $\bar{\mathbf{A}} = (\mathbf{A}_0 \mathbf{A}_0^*)^{-1/2} \mathbf{A}_0$. Concretely, if \mathbf{X}_0 is a sparse random matrix with independent symmetric entries [52], $\bar{\mathbf{Y}} = (\mathbf{Y} \mathbf{Y}^*)^{-1/2} \mathbf{Y} \approx c \bar{\mathbf{A}} \mathbf{X}_0$ satisfies a sparse model with orthogonal dictionary $\bar{\mathbf{A}}$, where $c > 0$ is a numerical constant. Similar to our discussion above, one can recover the columns of \mathbf{A}_0 by solving the optimization problem

$$\min \varphi(\mathbf{a}) \equiv h(\mathbf{a}^* \bar{\mathbf{Y}}) \quad \text{s. t.} \quad \mathbf{a} \in \mathbb{S}^{m-1}. \quad (3.12)$$

Although the columns of \mathbf{X}_0 are not one-sparse, when the number samples is large, this objective function retains all of the qualitative properties observed in the one-sparse problem, including local minimizers near symmetric solutions and saddle points near balanced superpositions of symmetric solutions, with negative curvature in symmetry breaking directions. The proofs of these properties rely heavily on probabilistic reasoning: one argues that the “population” objective function $\mathbb{E}_{\mathbf{X}_0} [\varphi]$ has benign structure, and then argues that when the number p of samples is large, gradients and Hessians of φ are uniformly close to those of $\mathbb{E}\varphi$, and hence φ has the same benign properties [20, 52].

Overcomplete Dictionary Learning In practice, *overcomplete* dictionaries, in which the number of dictionary atoms n is larger than the signal dimension m , are often favored compared to complete dictionaries. Overcomplete dictionaries have greater expressive power, yielding sparser coefficient matrices \mathbf{X}_0 . Our current theoretical understanding of the objective landscape associated with overcomplete dictionary learning is still developing. One suggestive result shows that when the dictionary is moderately overcomplete ($n \leq 3m$), under appropriate technical hypotheses, a formulation based on maximizing the ℓ^4 norm exhibits benign global geometry [53]: again, every local minimizer is global and saddle points exhibit strict negative curvature.²⁰ These results imply that overcomplete dictionary learning problems also exhibit benign global geometry. However, there are still a number of open questions around (i) the degree of overcompleteness n/m that this structure can tolerate and (ii) the extent to which similar properties hold in more conventional *synthesis* dictionary learning formulations, in which one optimizes over both \mathbf{A} and \mathbf{X} simultaneously.

3.3 Sparse Blind Deconvolution

Convolutional models arise in a wide range of problems in imaging and data analysis. The most basic convolutional data model expresses an observation \mathbf{y} as the convolution of two signals \mathbf{a}_0 and \mathbf{x}_0 . *Blind deconvolution* aims to recover \mathbf{a}_0 and \mathbf{x}_0 from the observation \mathbf{y} , up to certain intrinsic symmetries that we describe below. This problem is ill-posed in general – there are infinitely many $(\mathbf{a}_0, \mathbf{x}_0)$ that convolve to produce \mathbf{y} . To make progress, some low dimensional priors about \mathbf{a}_0 and \mathbf{x}_0 are essential. Different priors yield different nonconvex optimization problems; in this section, we will focus on several variants of blind deconvolution with sparsity priors on \mathbf{x}_0 , and then briefly mention other popular variants of blind deconvolution.

²⁰When the dictionary is overcomplete, dictionary atoms \mathbf{a}_i are correlated and $\mathbf{a}^* \bar{\mathbf{Y}}$ is no longer sparse, even if \mathbf{a} is chosen as one of the atoms \mathbf{a}_i . Rather, at $\mathbf{a} = \mathbf{a}_i$, $\mathbf{a}^* \bar{\mathbf{Y}}$ is *spiky*, with a few large entries amongst many small ones. ℓ^4 maximization is well-suited to encouraging this kind of spikiness. The most widely used practical dictionary learning algorithms are based on synthesis sparsity. Understanding the global geometry of this kind of formulation remains an important open problem

Short and Sparse Blind Deconvolution

Analyzing signals comprised of repeated motifs is a common task in areas such as neuroscience, materials science, astronomy, and natural and scientific imaging [57, 141–143]. Such signals can be modeled as the *convolution* of a short motif $\mathbf{a}_0 \in \mathbb{R}^k$ and a sparse coefficient signal $\mathbf{x}_0 \in \mathbb{R}^m$, which encodes occurring locations of the motif in time/space. Mathematically, the observation $\mathbf{y} \in \mathbb{R}^m$ is the windowed²¹ convolution of the short \mathbf{a}_0 , which is supported on k ($k \ll m$) consecutive entries, and the sparse \mathbf{x}_0 :

$$\mathbf{y} = \mathcal{P}_m [\mathbf{a}_0 * \mathbf{x}_0]. \quad (3.13)$$

Here, $*$ denotes linear convolution and $\mathcal{P}_m [\cdot]$ retains the entries supported on indices $0, \dots, m-1$.

The inverse problem of recovering \mathbf{a}_0 and \mathbf{x}_0 from \mathbf{y} is called *short and sparse blind deconvolution* (SaS-BD) [55, 56, 129]. The linear convolution $*$ exhibits a *signed shift symmetry*:

$$\mathbf{a}_0 * \mathbf{x}_0 = \alpha s_\tau [\mathbf{a}_0] * \alpha^{-1} s_{-\tau} [\mathbf{x}_0]. \quad (3.14)$$

Here α is some nonzero scalar and $s_\tau [\mathbf{v}]$ denotes a shift of vector \mathbf{v} by τ entries, i.e. $s_\tau [\mathbf{v}](i) = \mathbf{v}(i - \tau)$. As with the other nonconvex problems we have studied up to this point, we should expect this symmetry to play an critical role in shaping the landscape of optimization – in particular, we would expect the *global* minimizers to be symmetric copies of the ground truth.²²

Symmetry Breaking? However, there is a wrinkle: in order to obtain a finite dimensional optimization problem, one typically constrains the length- k signal \mathbf{a}_0 to be supported on $\{0, \dots, k-1\}$. This constraint appears to remove the shift symmetry: now only a scaled version ($\alpha \mathbf{a}_0, \alpha^{-1} \mathbf{x}_0$) of the truth exactly reproduces the observation. Perhaps surprisingly, even with this constraint, symmetry *still* shapes the landscape of optimization. However, instead of dictating the global minimizers, in constrained formulations, symmetry dictates the *local* minimizers. The reason is simple: a shift of \mathbf{a}_0 by τ samples is not supported on $\{0, \dots, k-1\}$, and hence is not feasible. Nonetheless, its truncation to $\{0, \dots, k-1\}$ is feasible, and still approximates \mathbf{y} :

$$\mathbf{y} \approx \mathcal{P}_k [s_\tau [\mathbf{a}_0]] * s_{-\tau} [\mathbf{x}_0]. \quad (3.15)$$

Because this approximation is not perfect, truncated shifts are *not* global minimizers, while they are very close to *local* minimizers [55, 129]. These points have suboptimal objective value and do not exactly reproduce $(\mathbf{a}_0, \mathbf{x}_0)$. Despite this, the optimization landscape is still sufficiently benign²³ that it is possible to exactly recover $(\mathbf{a}_0, \mathbf{x}_0)$ with efficient methods – one can, e.g., first find a local minimizer that is close to a truncated shift of \mathbf{a}_0 , and then refine it to exactly recover \mathbf{a}_0 [56, 129].

This problem illustrates how hard it is to avoid symmetry in studying deconvolution problems: even with an explicit symmetry breaking constraint, symmetry still shapes the landscape of optimization! The main motivation for studying this more complicated deconvolution model is its applicability. Giving formulations that better respect the symmetry structure, and hence have no spurious local minimizers, is an important open problem.

Multi-channel Sparse Blind Deconvolution

The problem of multi-channel sparse (MCS) blind deconvolution assumes access to *multiple* observations $\mathbf{y}_i = \mathcal{P}_m [\mathbf{a}_0 * \mathbf{x}_i]$ ($1 \leq i \leq n$) generated from n circular convolution²⁴ of $\mathbf{a}_0 \in \mathbb{R}^m$ and distinct sparse signals $\mathbf{x}_i \in \mathbb{R}^m$ [53, 58, 59, 144]. Here, shift symmetry becomes a *cyclic* shift symmetry: there exist m equivalent solutions corresponding to m different cyclic shifts. The resulting optimization landscape exhibits similar characteristics to that of complete dictionary learning, which we have described in Section 3.1 and Figure 9. In particular, any local minimizer is a scaled cyclic shift of the ground truth [58, 59, 144].

²¹Rather than having complete access to the convolved signal (which could be infinitely long), we observe m consecutive entries of it.

²²Notice that the scale and shift symmetries are intrinsic to the convolution operator in (3.13). Although we focus on *sparse* deconvolution, these symmetries will persist in deconvolution with any shift-invariant structural model for \mathbf{a}_0 and \mathbf{x}_0 . Moreover, as we will see below, they persist even in the presence of artificial symmetry-breaking mechanisms, in the sense that they still dictate the local minimizers.

²³In particular, there is negative curvature in symmetry breaking directions.

²⁴The linear convolution is a better model for many practical application. Despite this, there is no loss of generality as any statements about cyclic convolution, which can easily be carried over to linear convolution; by zero-padding \mathbf{x}_i appropriately, one can always rewrite a linear convolution as a cyclic convolution.

Geometry of Sparse Blind Deconvolution

Despite the technical differences of the convolution operator in MCS and SaS blind deconvolution problems, their optimization landscapes share the following key common phenomena:

- *Symmetric copies of the ground truth are minimizers.* The local minimizers are either a cyclic shifted or shifted truncation of the ground truth under conditions. Both can be viewed as a result of the inherent shift symmetry.
- *Negative curvature in symmetry breaking directions.* Near saddle points, there is negative curvature in the direction of any particular (truncated) shifted copy of the ground truth, and the objective value decreases by moving towards this symmetry breaking direction.
- *Cascade of saddle points.* The saddle points are approximately balanced superpositions of several shifts of the ground truth. The more shifts participate, the larger the objective value and the more negative eigenvalues the Hessian exhibits.

Other Blind Deconvolution Variants

Subspace Blind Deconvolution is another widely studied variant of blind deconvolution that leverages a low dimensional model for the pair $(\mathbf{a}_0, \mathbf{x}_0)$. In this variant, \mathbf{a}_0 and \mathbf{x}_0 are assumed to lie on known low-dimensional subspaces [145]. This problem can be cast as a rank-one matrix recovery problem, which exhibits a similar geometry to the problems studied in Section 2.

Convolutional Dictionary Learning extends the basic convolution model (3.13) by allowing for multiple basic motifs $\mathbf{a}_1, \dots, \mathbf{a}_N$ [146]. More precisely, we observe one or more signals of the form $\mathbf{y} = \sum_{i=1}^N \mathbf{a}_i * \mathbf{x}_i$, and the goal is to recover all the \mathbf{a}_i and \mathbf{x}_i . In addition to the symmetries inherited from the convolution operator, this problem processes an additional *permutation symmetry*: permuting the index i does not change the approximation to \mathbf{y} . Despite this additional complexity, empirically local minimizers remain symmetric copies of the ground truth [57, 129]; under certain technical hypotheses, one can prove that natural first order algorithms always recover one such symmetric copy [53].

3.4 Other Nonconvex Problems with Discrete Symmetry

Symmetric Tensor Decomposition Tensors can be regarded as high dimensional generalizations of matrices. Tensor decomposition problems find many applications in statistics, data science, and machine learning [147–150]. Although we can usually generalize algebraic notions from matrices to tensors, their counterpart in tensors are often not as well-behaved or easy to compute [147]. In fact, many natural tensor problems are NP-hard in the worst-case [151].

Nonetheless, recent results suggest that certain appealing special cases of tensor decomposition are tractable [22, 148, 150]. This is especially true for orthogonal tensor decomposition, where the task is to decompose a p -th order symmetric tensor (e.g., $p = 3, 4, \dots$) into these orthogonal components. More specifically, an orthogonal tensor \mathcal{T} with r components can be presented in the following form

$$\mathcal{T} = \sum_{k=1}^r \mathbf{a}_k^{\otimes p}, \quad r \leq n, \quad (3.16)$$

with $\{\mathbf{a}_k\}_{k=1}^r$ are a collection of orthogonal vectors, and $\mathbf{a}^{\otimes p}$ denotes the p -way outer product of a vector \mathbf{a} . The orthogonal tensor decomposition shares many similarities with the other nonconvex problems with discrete symmetry discussed above:

- the problem exhibits a *signed permutation symmetry* which is similar to dictionary learning: given \mathcal{T} we can only hope to recover the orthogonal components $\{\mathbf{a}_k\}_{k=1}^r$ up to an order permutation;
- whenever p is a number of even order, as shown in Figure 5, a natural nonconvex formulation

$$\min_{\mathbf{x} \in \mathbb{S}^{n-1}} -\mathcal{T}(\mathbf{x}, \dots, \mathbf{x}) = -\|\mathbf{A}^* \mathbf{x}\|_p^p \quad \text{with} \quad \mathbf{A} = [\mathbf{a}_1 \quad \dots \quad \mathbf{a}_r] \quad (3.17)$$

manifests a similar optimization landscape, for which every local minimizer is close to one of the signed orthogonal components and other critical points exhibit strict negative curvature.

These results have inspired further endeavors beyond orthogonal tensors [53, 60, 152]. One particular case of interest is decomposing a symmetric tensor \mathcal{T} in (3.16) with $r > n$ and nonorthogonal $\{\mathbf{a}_k\}_{k=1}^r$, which is often referred as *overcomplete* tensor decomposition. In particular, when $p = 4$, $r \in \mathcal{O}(n^{1.5})$ and $\{\mathbf{a}_k\}_{k=1}^r$ are i.i.d. Gaussian, [60] shows that (3.17) has no bad local minimizer over a level set whose measure geometrically shrinks w.r.t. the problem dimension; for $p = 4$, $r < 3n$, and incoherent $\{\mathbf{a}_k\}_{k=1}^r$, [53] presented a global analysis for overcomplete tensor decomposition, disclosing its connection to overcomplete dictionary learning. Nonetheless, these results are still far from providing a complete understanding of overcomplete tensor decomposition. One interesting question remains largely open is when bad local minimizers exist for large rank $r \gg n$ in the nonorthogonal case.

Clustering Clustering is one of the most fundamental problems in unsupervised learning. This problem possesses a *permutation symmetry*: one can generate equivalent clusters by permuting the indices for cluster centers. Popular nonconvex algorithms include the Lloyd algorithm and variants of Expectation-Maximization. Despite the broad applications and empirical success of these methods, few theoretical guarantees have been obtained until recently. The problem of demixing two balanced, identical data clusters manifests global convergence to (a symmetric copy of) the ground truth [41, 42, 153–155]. We see similar geometric properties hold here: *symmetric copies of the ground truth are minimizers and saddle points exhibit directions of strict negative curvature*. Moreover, the saddle points are also located at balanced superpositions of local minimizers. Sometimes, these saddle points may contain redundant cluster estimates. In this case, the redundant cluster estimates can be interpreted as an under-parametrized solution (with a smaller k specified).

However, in general, clustering problems with more than two clusters, local minimizers provably exist [156, 157]. When the clusters are sufficiently separated, these local minimizers possess characteristic structures [43]: they correspond to imbalanced segmentations of the data, in which a subset of the true clusters are optimally under-segmented and another subset is optimally over-segmented.

Fourier Phase Retrieval How to efficiently solve *Fourier* phase retrieval is a crucial problem in scientific imaging. In this problem, the goal is to recover \mathbf{x}_0 from observation $\mathbf{y} = |\mathcal{F}(\mathbf{x}_0)|$. Apart from the rotational (phase) symmetry, the problem of Fourier phase retrieval manifests two additional symmetries:²⁵ *(cyclic)-shift symmetry* $|\mathcal{F}(\mathbf{x})| = |\mathcal{F}(s_\tau[\mathbf{x}])|$ and *conjugate inversion symmetry* $|\mathcal{F}(\mathbf{x})| = |\mathcal{F}(\tilde{\mathbf{x}})|$, where $\tilde{\mathbf{x}}(n) = \bar{\mathbf{x}}(-n)$ [158]. This complicated symmetry structure is reflected in a complicated optimization landscape, which is challenging to study analytically. Many basic problems in the algorithmic theory of Fourier phase retrieval remain open.

4 Discussion

Finally, we conclude this review by pointing several important future directions. We start with a discussion on training deep neural networks. We show how the symmetry and geometry can play crucial roles in analyzing some interesting phenomena in deep learning. Second, we conclude by touching some important generic questions in nonconvex optimization, such as relationship to convexification, development of more unified theory, and more efficient optimization methods.

4.1 Symmetry & Geometry in Training Deep Neural Networks

In the past decade, the revival of deep neural networks (DNN) has led to dramatic success in numerous applications ranging from computer vision, to natural language processing, to scientific discovery and beyond [7, 159–161]. However, because most neural network learning problems are highly nonconvex, to date a deep network is still viewed as a *black-box* and the practice of deep networks has been shrouded with mystery.

Taking the multi-class (say K classes) classification problem for an example, the goal of deep network training is to learn a classifier \mathbf{W} and deep hierarchical representation (or feature) $\mathbf{h}(\mathbf{x})$, such that the output

²⁵When \mathbf{x} is one dimensional, the problem becomes even more pessimistic — there exist multiple one dimensional signals with the same Fourier magnitude, but not related by an obvious symmetry.

$\psi(\mathbf{x}) = \mathbf{W}\mathbf{h}(\mathbf{x})$ of the network fits the input \mathbf{x} to the corresponding (one-hot) training label \mathbf{y} . In the vanilla form, a L -layer neural network can be written as

$$\psi_{\Theta}(\mathbf{x}_{i,k}) = \underbrace{\mathbf{W}_L}_{\text{linear classifier } \mathbf{W}} \cdot \sigma(\underbrace{\mathbf{W}_{L-1} \cdots \sigma(\mathbf{W}_1 \mathbf{x}_{i,k} + \mathbf{b}_1)}_{\text{feature } \mathbf{h}_{i,k} = \phi_{\Theta}(\mathbf{x}_{i,k})} + \mathbf{b}_{L-1}) + \mathbf{b}_L, \quad (4.1)$$

where each layer is composed of an affine transformation, represented by some weight matrix \mathbf{W}_{ℓ} , and bias \mathbf{b}_{ℓ} , followed by a nonlinear activation function $\sigma(\cdot)$, and $\Theta = \{\mathbf{W}_{\ell}, \mathbf{b}_{\ell}\}_{\ell=1}^L$ denotes the network parameters. To learn those weight parameters Θ , one typically minimizes an empirical risk over training samples of the following form

$$\min_{\Theta} \sum_{k=1}^K \sum_{i=1}^n L(\psi_{\Theta}(\mathbf{x}_{k,i}), \mathbf{y}_k) + \frac{\lambda}{2} \|\Theta\|_F^2, \quad (4.2)$$

where $\mathbf{y}_k \in \mathbb{R}^K$ is a one-hot vector with only the k th entry equal to unity ($1 \leq k \leq K$), n are the numbers of training samples in each class,²⁶ and $\lambda > 0$ is the regularization parameter (or weight decay penalty), and $L(\cdot, \cdot)$ is a data fidelity term (e.g., cross entropy loss). As we observe from (4.1), deep neural networks typically exhibit complicated symmetries which include compositions of permutations, and nonlinear interactions between layers, so that the training loss (4.2) is highly nonconvex. This formulation can be naturally generalized from classification to regression problems. Studying the nonconvex optimization landscape in neural network training has been an active research area recently; see [162–167] for contemporary surveys.

Study of Multi-layer Linear Neural Network To simplify the problem, people considered *linear* neural networks by removing all nonlinear activation $\sigma(\cdot)$ in (4.1) as a more approachable object of theoretical investigation. This model exhibits rotational symmetries at each layer. Using similar considerations to those described in Section 2.3 for low-rank matrix factorization, the line of work [33, 168–171] studied the optimization landscape for linear two-layer networks and proved that the associated training loss is a strict saddle function. As with matrix factorization, critical points of natural optimization models correspond to “underfactorizations”. Additionally, some related works study the learning dynamics of gradient descent [172, 173]. For deeper linear networks, however, in contrast to matrix factorization, this problem does possess “flat” saddle points at which the Hessian has no negative eigenvalues – this is the result of the compound effect of symmetries at multiple layers, but there are no spurious local minima [33, 174]. Nonetheless, because the power of deep neural network originates from its nonlinearity, the removal of the nonlinear interaction makes linear deep neural networks far from practice.

Study of Nonlinear Neural Network When the nonlinear activations in (4.1) are considered, the problem has more complicated symmetry groups than the problems described above. For example, natural objective functions associated with fitting a fully connected neural network are invariant under simultaneous permutations of the features at *each* layer. We currently lack tools for reasoning about the global geometry of such problems. However, progress has been made on certain special cases: for example, certain problems associated with fitting shallow networks share similar geometry to tensor decomposition [175, 176]. With varying technical assumptions, all local solutions have been shown to be global in a 1-layer neural network [34, 177–180]. However, general deep nonlinear neural networks can exhibit flat saddles and spurious local minimizers for all the weight parameters [162, 181, 182], but such local minima may be eliminated, or the number can be significantly reduced, in the over-parameterization regime [183, 184]. Additionally, the work [185] proved that certain local minima (having an all-zero “slice”) are also global solutions, but the analysis is crucially dependent on the sufficient condition of an all-zero slice in the weights, which is insufficient to characterize the landscape properties.

Investigation Under Simplified Unconstrained Feature Model To avoid the challenges on dealing with nonlinear interactions across layers, recent works simplify the study of deep network (4.1) by assuming a certain *unconstrained feature model* (UFM) [186–194] and investigate the structure of last-layer representations – by making an assumption that the representation $\mathbf{h}_{i,k}$ of each input $\mathbf{x}_{i,k}$ in (4.1) is a *free* optimization variable,

²⁶For simplicity, we assume balanced class, that each class has the same number of training samples.

we can avoid the nonlinear interactions between layers and reduce the problem similar to matrix factorization with *only* the rotational symmetry. The underlying motivation behind UFM is that modern neural networks are highly overparameterized to approximate any continuous function [195–198]. Thus, based upon the UFM, recent work [192, 194] reduced (4.2) to much simpler optimization problems such as the following

$$\min_{\mathbf{W}, \mathbf{H}, \mathbf{b}} f(\mathbf{W}, \mathbf{H}, \mathbf{b}) := \frac{1}{Kn} \sum_{k=1}^K \sum_{i=1}^n L(\mathbf{W} \mathbf{h}_{k,i} + \mathbf{b}, \mathbf{y}_k) + \frac{\lambda_{\mathbf{W}}}{2} \|\mathbf{W}\|_F^2 + \frac{\lambda_{\mathbf{H}}}{2} \|\mathbf{H}\|_F^2 + \frac{\lambda_{\mathbf{b}}}{2} \|\mathbf{b}\|_2^2, \quad (4.3)$$

with $\mathbf{W} \in \mathbb{R}^{K \times d}$, $\mathbf{H} = [\mathbf{h}_{1,1} \cdots \mathbf{h}_{K,n}] \in \mathbb{R}^{d \times N}$ (here, we denote $N = nK$), $\mathbf{b} \in \mathbb{R}^K$, and $\lambda_{\mathbf{W}}, \lambda_{\mathbf{H}}, \lambda_{\mathbf{b}} > 0$ are the penalty parameters. The difference of (4.3) from (4.2) is that the regularization is on \mathbf{W} and \mathbf{H} instead of all network parameters Θ . Recent work [192–194] showed that the nonconvex objective (4.3) exhibits similar symmetry and geometric structure as the low-rank matrix recovery that we discussed in Section 2.3. While all saddle points of (4.3) are also strict saddles whose Hessian exhibit negative curvature directions, the minor differences lie in the global solutions. Because of the particular structure of the one-hot encoders \mathbf{y}_k , the only global solutions of (4.3) are more structured – they satisfies certain properties termed *Neural Collapse* (\mathcal{NC}) [199, 200]. This phenomenon has been empirically revealed as well for training practical deep networks [199, 200], that (i) the class means and the last-layer classifiers all collapse to the vertices of a Simplex Equiangular Tight Frame (ETF) up to scaling, and (ii) cross-example within-class variability of last-layer representations collapses to zero. Under the UFM assumption, recent works showed that the global optimality and \mathcal{NC} happen for a variety of loss function $L(\cdot)$, such as cross-entropy [187, 189, 192, 193, 199], mean-squared error [186, 194, 200, 201], and supervised contrastive loss [190]. Moreover, the simplified analysis based upon UFM not only characterizes the features that are learned in the last layer, but also explains why they can be efficiently optimized. The study of symmetry and geometry provides theoretical support for empirical observations in practical deep network architectures.

Although it sounds plausible, however, it should be noted that the presented global landscape analysis in [192–194] is *only* with respect to the last-layer feature \mathbf{H} and classifier \mathbf{W} , *not* the network parameters Θ . For deep network training, it should be noted that spurious local minima *do exist* for Θ [37, 183], and the training algorithm often has implicit bias towards certain low-dimensional solutions [173, 202–204].

4.2 Methodological Points & Future Directions

This work has reviewed recent advances in provable nonconvex methods for signal processing and machine learning, through the lens of symmetry and geometry. It is an exciting time to work on both the theory and practice of nonconvex optimization. For complementary perspectives on the area, we refer interested readers to other recent review papers [10–12, 63]. In the following, we close by discussing several general methodological points and general directions for future work.

Convexification In the past decades, convex relaxation has been demonstrated a powerful tool for solving nonconvex problems such as sparse recovery [205, 206] low-rank matrix completion [101, 115, 207], etc. For these problems, convex relaxation achieves near-optimal sample complexity. Which nonconvex problems are amenable to convex relaxation? There are general results that suggest that *unimodal* functions (i.e., functions with one local minimizer) on convex sets can be convexified, by endowing the space with an appropriate geometry [208].²⁷ The symmetric problems encountered in this survey are not unimodal. The degree to which they are amenable to convex relaxation varies substantially:

- **Problems with rotational symmetry.** Many problems with rotational symmetry *can* be convexified by lifting to a higher dimensional space [68, 101, 115], e.g., by replacing the factor \mathbf{U} with a matrix valued variable $\mathbf{X} = \mathbf{U}\mathbf{U}^*$. This collapses the $O(r)$ symmetry; the resulting problems can often be converted to semidefinite programs and solved globally. Typically, nonconvex formulations are still preferred in practice, due to their scalability to large datasets. Section 2 and the references therein describe alternative geometric principles that help to explain the success of these methods.

²⁷These are existence results; their direct implications for efficient computation are limited, since they apply to NP-hard problems. It is also worth noting that many of our discrete symmetric problems in Section 3 are formulated over compact manifolds such as \mathbb{S}^{n-1} ; the only continuous geodesically convex function on a compact Riemannian manifold is a constant [209, 210].

- **Problems with discrete symmetry.** Most of the discrete symmetric problems described in Section 3 do not admit simple convex relaxations. For example, complete dictionary learning can be reduced to a sequence of linear programs [132], but only in the highly sparse case, in which the target sparse representation has $O(\sqrt{n})$ nonzero entries per length- n data vector. These limitations are attributable in part to the more complicated discrete symmetry structure. Natural ideas, such as taking a quotient by the symmetry group, encounter obstacles at both the conceptual and implementation levels. One general methodology which *does* meet with success in this setting is sum-of-squares relaxation, which for variants of dictionary learning and tensor decomposition leads to quasipolynomial or even polynomial-time algorithms [211].

Disciplined Formulations and Analysis Our understanding of nonconvex optimization is still far from satisfactory – analyses are delicate, case-by-case, and pertain to problems with elementary symmetry (e.g., rotation or permutation) and simple constraints (e.g., the sphere).

- **A unified theory for nonconvex optimization.** Analogous to the study of convex functions [212], there is a pressing need for simpler analytic tools, to identify and generalize benign properties for new nonconvex problems, despite some recent endeavors [53, 130] of identifying general conditions and operations preserving benign geometric structures.
- **Coping with complicated symmetries and constraints.** Practical nonconvex problems often involve *multiple symmetries* (e.g., Fourier phase retrieval and deep neural networks) and/or *complicated manifolds* (e.g., the Stiefel manifold [40]). We need better technical tools to understand the impact of compound symmetries (especially compound discrete symmetries) on the optimization landscape, despite some steps in this directions [40, 128, 130].
- **Dealing with nonsmoothness.** In many scenarios we encounter nonconvex problems with *nonsmooth* formulations [118, 119, 126, 130, 213–216], for better promoting solution sparsity or robustness. However, most of our current analysis is local [130, 216], and (subgradient) optimization [126, 130, 215, 217] could be slow to converge. Attempts to obtain global analyses and fast optimization methods might benefit from more sophisticated tools from variational analysis [218] and development of efficient 2nd-order methods [93].

Efficient First-Order Algorithms In this paper, we have described families of symmetric nonconvex optimization problems with benign global geometry: local minimizers are global and saddle points exhibit strict negative curvature. Although we have not emphasized algorithmic aspects of these problems, this geometric structure *does* have strong implications for computation – a variety of methods the key is leveraging negative curvature to efficiently obtain minimizers. One class of methods explicitly models negative curvature, e.g., using a second-order approximation to the objective function. Methods in this class include trust-region methods [19], cubic regularization [25], and curvilinear search [24]. These methods can be challenging to scale to very large problems, since they typically require computation and storage of the Hessian. It is also possible to leverage negative curvature using more scalable first-order methods such as gradient descent. In the vicinity of a saddle point, the gradient method essentially performs a power iteration that moves in directions of negative curvature. Although this scheme *can* stagnate at or near saddle points, it is possible to guarantee efficient escape by perturbing the iterates with an appropriate amount of random noise [22, 26, 30, 219, 220].

The methods described above are efficient across the broad class of *strict saddle functions* [9, 22], i.e., functions whose saddle points all have directions of strict negative curvature. This is a worst case performance guarantee. Perhaps surprisingly, the simplest and most widely used first order method, gradient descent, is not efficient for worst case strict saddle functions: although randomly initialized gradient descent *does* obtain a minimizer with probability one [21, 27], for certain strict saddle functions it can take time exponential in dimension [221]. These challenging functions have a large numbers of saddle points, which are conspicuously arranged such that upstream negative curvature directions align with *positive* curvature directions for downstream saddle points.

This worst case behavior is in some sense the opposite of what is observed in the type of highly symmetric functions studied here: functions encountered in generalized phase retrieval [222], dictionary learning [45], deconvolution [59, 144], etc., exhibit a global negative curvature structure ([45] and Appendix B, in which

upstream negative curvature directions align with *negative* curvature directions of downstream saddle points. In this situation, randomly initialized gradient descent is efficient. This points to another gap between naturally occurring nonconvex optimization problems and their worst case counterparts. There is substantial room for future work in this direction.

Acknowledgement

This work was supported by the grants NSF CCF 1527809, NSF CCF 1740833, NSF CCF 1733857, and NSF IIS 1546411. YZ acknowledges support from Electrical and Computer Engineering Department at Rutgers University. QQ acknowledges past support from Microsoft Ph.D. fellowship, Moore-Sloan fellowship, and the grant NSF DMS 2009752 for conducting part of the research, and also acknowledges current funding support from U-M START & PODS grants, NSF CAREER CCF 2143904, NSF CCF 2212066, NSF CCF 2212326, and ONR N00014-22-1-2529. We also thank our colleagues Jun Sun (University of Minnesota), Yuxin Chen (University of Pennsylvania), Yi Ma (UC Berkeley), Zhihui Zhu (University of Denver), Sam Buchanan (Columbia University), Han-wen Kuo (Google) for discussion and contributions on related works.

References

- [1] A. L. Patterson, "A fourier series method for the determination of the components of interatomic distances in crystals," *Physical Review*, vol. 46, no. 5, p. 372, 1934.
- [2] A. L. Patterson, "Ambiguities in the x-ray analysis of crystal structures," *Physical Review*, vol. 65, no. 5-6, p. 195, 1944.
- [3] Y. Shechtman, Y. C. Eldar, O. Cohen, H. N. Chapman, J. Miao, and M. Segev, "Phase retrieval with application to optical imaging: a contemporary overview," *IEEE Signal Processing Magazine*, vol. 32, no. 3, pp. 87–109, 2015.
- [4] K. Jaganathan, Y. C. Eldar, and B. Hassibi, "Phase retrieval: An overview of recent developments," *Optical Compressive Imaging*, pp. 263–296, 2017.
- [5] Y. LeCun and Y. Bengio, "Convolutional networks for images, speech, and time series," 1995.
- [6] I. Goodfellow, J. Pouget-Abadie, M. Mirza, B. Xu, D. Warde-Farley, S. Ozair, A. Courville, and Y. Bengio, "Generative adversarial nets," in *Advances in neural information processing systems*, pp. 2672–2680, 2014.
- [7] I. Goodfellow, Y. Bengio, and A. Courville, *Deep learning*. MIT press, 2016.
- [8] A. Cauchy, "Méthode générale pour la résolution des systemes d'équations simultanées,"
- [9] J. Sun, Q. Qu, and J. Wright, "When are nonconvex problems not scary?," *arXiv preprint arXiv:1510.06096*, 2015.
- [10] P. Jain, P. Kar, *et al.*, "Non-convex optimization for machine learning," *Foundations and Trends® in Machine Learning*, vol. 10, no. 3-4, pp. 142–336, 2017.
- [11] Y. Chi, Y. M. Lu, and Y. Chen, "Nonconvex optimization meets low-rank matrix factorization: An overview," *IEEE Transactions on Signal Processing*, vol. 67, no. 20, pp. 5239–5269, 2019.
- [12] J. Sun, "Provable nonconvex methods/algorithms." <https://sunju.org/research/nonconvex/>.
- [13] K. G. Murty and S. N. Kabadi, "Some NP-complete problems in quadratic and nonlinear programming," *Mathematical programming*, vol. 39, no. 2, pp. 117–129, 1987.
- [14] Y. Nesterov, "Squared functional systems and optimization problems," in *High performance optimization*, pp. 405–440, Springer, 2000.
- [15] M. A. Erdogdu, L. Mackey, and O. Shamir, "Global non-convex optimization with discretized diffusions," in *Advances in Neural Information Processing Systems*, pp. 9671–9680, 2018.
- [16] P. Hajela, "Genetic search-an approach to the nonconvex optimization problem," *AIAA journal*, vol. 28, no. 7, pp. 1205–1210, 1990.
- [17] J. V. Burke, A. S. Lewis, and M. L. Overton, "A robust gradient sampling algorithm for nonsmooth, nonconvex optimization," *SIAM Journal on Optimization*, vol. 15, no. 3, pp. 751–779, 2005.
- [18] P.-A. Absil, C. G. Baker, and K. A. Gallivan, "Trust-region methods on Riemannian manifolds," *Foundations of Computational Mathematics*, vol. 7, no. 3, pp. 303–330, 2007.
- [19] A. R. Conn, N. I. Gould, and P. L. Toint, *Trust region methods*, vol. 1. SIAM, 2000.
- [20] J. Sun, Q. Qu, and J. Wright, "Complete dictionary recovery over the sphere ii: Recovery by riemannian trust-region method," *IEEE Transactions on Information Theory*, vol. 63, no. 2, pp. 885–914, 2017.
- [21] J. D. Lee, M. Simchowitz, M. I. Jordan, and B. Recht, "Gradient descent only converges to minimizers," in *Conference on Learning Theory*, pp. 1246–1257, 2016.
- [22] R. Ge, F. Huang, C. Jin, and Y. Yuan, "Escaping from saddle points—online stochastic gradient for tensor decomposition," in *Proceedings of The 28th Conference on Learning Theory*, pp. 797–842, 2015.
- [23] C. Jin, P. Netrapalli, R. Ge, S. M. Kakade, and M. I. Jordan, "On nonconvex optimization for machine learning: Gradients, stochasticity, and saddle points," *Journal of the ACM (JACM)*, vol. 68, no. 2, pp. 1–29, 2021.
- [24] D. Goldfarb, "Curvilinear path steplength algorithms for minimization which use directions of negative curvature," *Mathematical programming*, vol. 18, no. 1, pp. 31–40, 1980.

- [25] Y. Nesterov and B. T. Polyak, "Cubic regularization of newton method and its global performance," *Mathematical Programming*, vol. 108, no. 1, pp. 177–205, 2006.
- [26] C. Jin, P. Netrapalli, and M. I. Jordan, "Accelerated gradient descent escapes saddle points faster than gradient descent," in *Conference On Learning Theory*, pp. 1042–1085, 2018.
- [27] J. D. Lee, I. Panageas, G. Piliouras, M. Simchowitz, M. I. Jordan, and B. Recht, "First-order methods almost always avoid strict saddle points," *Mathematical programming*, vol. 176, no. 1-2, pp. 311–337, 2019.
- [28] J. Milnor, *Morse theory.(AM-51)*, vol. 51. Princeton university press, 2016.
- [29] R. Bott, "Lectures on morse theory, old and new," *Bulletin of the american mathematical society*, vol. 7, no. 2, pp. 331–358, 1982.
- [30] C. Jin, R. Ge, P. Netrapalli, S. M. Kakade, and M. I. Jordan, "How to escape saddle points efficiently," in *34th International Conference on Machine Learning, ICML 2017*, pp. 2727–2752, International Machine Learning Society (IMLS), 2017.
- [31] J. D. Lee, I. Panageas, G. Piliouras, M. Simchowitz, M. I. Jordan, and B. Recht, "First-order methods almost always avoid saddle points," *arXiv preprint arXiv:1710.07406*, 2017.
- [32] A. Choromanska, M. Henaff, M. Mathieu, G. B. Arous, and Y. LeCun, "The loss surface of multilayer networks," *arXiv preprint arXiv:1412.0233*, 2014.
- [33] K. Kawaguchi, "Deep learning without poor local minima," in *Advances in neural information processing systems*, pp. 586–594, 2016.
- [34] M. Soltanolkotabi, A. Javanmard, and J. D. Lee, "Theoretical insights into the optimization landscape of over-parameterized shallow neural networks," *IEEE Transactions on Information Theory*, vol. 65, no. 2, pp. 742–769, 2018.
- [35] Z. Allen-Zhu, Y. Li, and Z. Song, "A convergence theory for deep learning via over-parameterization," in *International Conference on Machine Learning*, pp. 242–252, 2019.
- [36] S. Du, J. Lee, H. Li, L. Wang, and X. Zhai, "Gradient descent finds global minima of deep neural networks," in *International Conference on Machine Learning*, pp. 1675–1685, 2019.
- [37] R. Sun, "Optimization for deep learning: theory and algorithms," *arXiv preprint arXiv:1912.08957*, 2019.
- [38] A. Kyrillidis, A. Kalev, D. Park, S. Bhojanapalli, C. Caramanis, and S. Sanghavi, "Provable compressed sensing quantum state tomography via non-convex methods," *npj Quantum Information*, vol. 4, no. 1, pp. 1–7, 2018.
- [39] F. Sheldon, F. L. Traversa, and M. Di Ventra, "Taming a non-convex landscape with dynamical long-range order: memcomputing the ising spin-glass," *arXiv preprint arXiv:1810.03712*, 2018.
- [40] J. Hu, X. Liu, Z. Wen, and Y. Yuan, "A brief introduction to manifold optimization," 2019.
- [41] W. Qian, Y. Zhang, and Y. Chen, "Global convergence of least squares EM for demixing two log-concave densities," in *Advances in Neural Information Processing Systems*, pp. 4795–4803, 2019.
- [42] J. Kwon, W. Qian, C. Caramanis, Y. Chen, and D. Davis, "Global convergence of the EM algorithm for mixtures of two component linear regression," in *Conference on Learning Theory*, pp. 2055–2110, 2019.
- [43] W. Qian, Y. Zhang, and Y. Chen, "Structures of spurious local minima in k -means," 2020.
- [44] K. Wang, Y. Yan, and M. Diaz, "Efficient clustering for stretched mixtures: Landscape and optimality," 2020.
- [45] D. Gilboa, S. Buchanan, and J. Wright, "Efficient dictionary learning with gradient descent," *ICML*, 2019.
- [46] E. J. Candès, Y. C. Eldar, T. Strohmer, and V. Voroninski, "Phase retrieval via matrix completion," *SIAM Journal on Imaging Sciences*, vol. 6, no. 1, 2013.
- [47] E. J. Candès, X. Li, and M. Soltanolkotabi, "Phase retrieval via wirtinger flow: Theory and algorithms," *IEEE Transactions on Information Theory*, vol. 61, no. 4, pp. 1985–2007, 2015.
- [48] J. Sun, Q. Qu, and J. Wright, "A geometric analysis of phase retrieval," *Foundations of Computational Mathematics*, vol. 18, no. 5, pp. 1131–1198, 2018.

- [49] A. Fannjiang and T. Strohmer, "The numerics of phase retrieval," 2020.
- [50] R. Ge, J. D. Lee, and T. Ma, "Matrix completion has no spurious local minimum," *arXiv preprint arXiv:1605.07272*, 2016.
- [51] R. Ge, C. Jin, and Y. Zheng, "No spurious local minima in nonconvex low rank problems: A unified geometric analysis," in *Proceedings of the 34th International Conference on Machine Learning*, pp. 1233–1242, 2017.
- [52] J. Sun, Q. Qu, and J. Wright, "Complete dictionary recovery over the sphere i: Overview and geometric picture," *IEEE Transactions on Information Theory*, vol. 63, no. 2, 2017.
- [53] Q. Qu, Y. Zhai, X. Li, Y. Zhang, and Z. Zhu, "Analysis of the optimization landscapes for overcomplete representation learning," *arXiv preprint arXiv:1912.02427*, 2019.
- [54] S. Ling and T. Strohmer, "Blind deconvolution meets blind demixing: Algorithms and performance bounds," *IEEE Transactions on Information Theory*, vol. 63, no. 7, pp. 4497–4520, 2017.
- [55] Y. Zhang, H.-W. Kuo, and J. Wright, "Structured local minima in sparse blind deconvolution," in *Advances in Neural Information Processing Systems 31*, pp. 2328–2337, 2018.
- [56] H.-W. Kuo, Y. Zhang, Y. Lau, and J. Wright, "Geometry and symmetry in short-and-sparse deconvolution," *arXiv preprint arXiv:1901.00256*, vol. 63, no. 7, pp. 4497–4520, 2019.
- [57] Y. Lau, Q. Qu, H.-W. Kuo, P. Zhou, Y. Zhang, and J. Wright, "Short-and-sparse deconvolution – a geometric approach," *Preprint*, 2019.
- [58] Y. Li and Y. Bresler, "Global geometry of multichannel sparse blind deconvolution on the sphere," *arXiv preprint arXiv:1805.10437*, 2018.
- [59] Q. Qu, X. Li, and Z. Zhu, "A nonconvex approach for exact and efficient multichannel sparse blind deconvolution," in *Advances in Neural Information Processing Systems*, pp. 4017–4028, 2019.
- [60] R. Ge and T. Ma, "On the optimization landscape of tensor decompositions," *Advances in Neural Information Processing Systems*, 2017.
- [61] Y. Chen and Y. Chi, "Harnessing structures in big data via guaranteed low-rank matrix estimation: Recent theory and fast algorithms via convex and nonconvex optimization," *IEEE Signal Processing Magazine*, vol. 35, no. 4, pp. 14–31, 2018.
- [62] Y. Chi, Y. M. Lu, and Y. Chen, "Nonconvex optimization meets low-rank matrix factorization: An overview," *arXiv preprint arXiv:1809.09573*, 2018.
- [63] Q. Qu, Z. Zhu, X. Li, M. C. Tsakiris, J. Wright, and R. Vidal, "Finding the sparsest vectors in a subspace: Theory, algorithms, and applications," *arXiv preprint arXiv:2001.06970*, 2020.
- [64] J. Hu, X. Liu, Z.-W. Wen, and Y.-X. Yuan, "A brief introduction to manifold optimization," *Journal of the Operations Research Society of China*, vol. 8, no. 2, pp. 199–248, 2020.
- [65] J. H. Manton, "Geometry, manifolds, and nonconvex optimization: How geometry can help optimization," *IEEE Signal Processing Magazine*, vol. 37, no. 5, pp. 109–119, 2020.
- [66] M. Danilova, P. Dvurechensky, A. Gasnikov, E. Gorbunov, S. Guminov, D. Kamzolov, and I. Shibaev, "Recent theoretical advances in non-convex optimization," *arXiv preprint arXiv:2012.06188*, 2020.
- [67] N. Boumal, "An introduction to optimization on smooth manifolds." To appear with Cambridge University Press, Apr 2022.
- [68] E. J. Candès, T. Strohmer, and V. Voroninski, "Phaselift: Exact and stable signal recovery from magnitude measurements via convex programming," *Communications on Pure and Applied Mathematics*, vol. 66, no. 8, pp. 1241–1274, 2013.
- [69] J. Miao, T. Ishikawa, B. Johnson, E. H. Anderson, B. Lai, and K. O. Hodgson, "High resolution 3d x-ray diffraction microscopy," *Physical Review Letters*, vol. 89, no. 8, p. 088303, 2002.

- [70] O. Bunk, A. Diaz, F. Pfeiffer, C. David, B. Schmitt, D. K. Satapathy, and J. F. van der Veen, "Diffractive imaging for periodic samples: retrieving one-dimensional concentration profiles across microfluidic channels," *Acta Crystallographica Section A*, vol. 63, pp. 306–314, Jul. 2007.
- [71] A. Chai, M. Moscoso, and G. Papanicolaou, "Array imaging using intensity-only measurements," *Inverse Problems*, vol. 27, no. 1, p. 015005, 2010.
- [72] R. Balana, P. Casazzab, and D. Edidin, "On signal reconstruction without phase," *Applied and Computational Harmonic Analysis*, vol. 20, no. 3, pp. 345 – 356, 2006.
- [73] R. V. Balan, "On signal reconstruction from its spectrogram," in *Information Sciences and Systems (CISS), 44th Annual Conference on*, pp. 1–4, IEEE, 2010.
- [74] J. V. Corbett, "The pauli problem, state reconstruction and quantum-real numbers," *Reports on Mathematical Physics*, vol. 57, no. 1, pp. 53–68, 2006.
- [75] H. Reichenbach in *Philosophic foundations of quantum mechanics*, University of California Press, 1965.
- [76] T. Heinosaari, L. Mazzarella, and M. M. Wolf, "Quantum tomography under prior information," *Communications in Mathematical Physics*, vol. 318, no. 2, pp. 355–374, 2013.
- [77] R. P. Millane, "Phase retrieval in crystallography and optics," *Journal of the Optical Society of America A*, vol. 7, pp. 394–411, Mar 1990.
- [78] W. H. Robert, "Phase problem in crystallography," *Journal of the Optical Society of America A*, vol. 10, no. 5, pp. 1046–1055, 1993.
- [79] A. Walther, "The question of phase retrieval in optics," *Journal of Modern Optics*, vol. 10, no. 1, pp. 41–49, 1963.
- [80] C. Dainty and J. R. Fienup, "Phase retrieval and image reconstruction for astronomy," *Image Recovery: Theory and Application*, pp. 231–275, 1987.
- [81] J. R. Fienup, "Phase retrieval algorithms: a personal tour," *Applied optics*, vol. 52, no. 1, pp. 45–56, 2013.
- [82] K. Jaganathan, Y. C. Eldar, and B. Hassibi, "Phase retrieval: An overview of recent developments," *arXiv preprint arXiv:1510.07713*, 2015.
- [83] E. J. Candès, X. Li, and M. Soltanolkotabi, "Phase retrieval from coded diffraction patterns," *Applied and Computational Harmonic Analysis*, vol. 39, no. 2, pp. 277–299, 2015.
- [84] L.-H. Yeh, J. Dong, J. Zhong, L. Tian, M. Chen, G. Tang, M. Soltanolkotabi, and L. Waller, "Experimental robustness of fourier ptychography phase retrieval algorithms," *Optics express*, vol. 23, no. 26, pp. 33214–33240, 2015.
- [85] K. Jaganathan, Y. C. Eldar, and B. Hassibi, "Stft phase retrieval: Uniqueness guarantees and recovery algorithms," *IEEE Journal of selected topics in signal processing*, vol. 10, no. 4, pp. 770–781, 2016.
- [86] F. Pfeiffer, "X-ray ptychography," *Nature Photonics*, vol. 12, no. 1, pp. 9–17, 2018.
- [87] L. Tian and L. Waller, "3d intensity and phase imaging from light field measurements in an led array microscope," *optica*, vol. 2, no. 2, pp. 104–111, 2015.
- [88] M. R. Kellman, E. Bostan, N. A. Repina, and L. Waller, "Physics-based learned design: optimized coded-illumination for quantitative phase imaging," *IEEE Transactions on Computational Imaging*, vol. 5, no. 3, pp. 344–353, 2019.
- [89] Y. Chen and E. J. Candès, "Solving random quadratic systems of equations is nearly as easy as solving linear systems," *Communications on pure and applied mathematics*, vol. 70, no. 5, pp. 822–883, 2017.
- [90] I. Waldspurger, A. d'Aspremont, and S. Mallat, "Phase recovery, maxcut and complex semidefinite programming," *Mathematical Programming*, vol. 149, no. 1-2, pp. 47–81, 2015.
- [91] C. Ma, K. Wang, Y. Chi, and Y. Chen, "Implicit regularization in nonconvex statistical estimation: Gradient descent converges linearly for phase retrieval, matrix completion and blind deconvolution," *arXiv preprint arXiv:1711.10467*, 2017.
- [92] G. Wang, G. B. Giannakis, and Y. C. Eldar, "Solving systems of random quadratic equations via truncated amplitude flow," *IEEE Transactions on Information Theory*, vol. 64, no. 2, pp. 773–794, 2017.

- [93] J. C. Duchi and F. Ruan, "Solving (most) of a set of quadratic equalities: Composite optimization for robust phase retrieval," *Information and Inference: A Journal of the IMA*, vol. 8, no. 3, pp. 471–529, 2019.
- [94] D. Davis, D. Drusvyatskiy, and C. Paquette, "The nonsmooth landscape of phase retrieval," *arXiv preprint arXiv:1711.03247*, 2017.
- [95] Z. Li, K. Lange, and J. A. Fessler, "Algorithms for poisson phase retrieval," *arXiv preprint arXiv:2104.00861*, 2021.
- [96] Q. Qu, Y. Zhang, Y. Eldar, and J. Wright, "Convolutional phase retrieval," in *Advances in Neural Information Processing Systems*, pp. 6086–6096, 2017.
- [97] P. Grohs, S. Koppensteiner, and M. Rathmair, "Phase retrieval: uniqueness and stability," *SIAM Review*, vol. 62, no. 2, pp. 301–350, 2020.
- [98] M. A. Davenport and J. Romberg, "An overview of low-rank matrix recovery from incomplete observations," *IEEE Journal of Selected Topics in Signal Processing*, vol. 10, no. 4, pp. 608–622, 2016.
- [99] S. Burer and R. D. Monteiro, "A nonlinear programming algorithm for solving semidefinite programs via low-rank factorization," *Mathematical Programming*, vol. 95, no. 2, pp. 329–357, 2003.
- [100] X. Li, J. Lu, R. Arora, J. Haupt, H. Liu, Z. Wang, and T. Zhao, "Symmetry, saddle points, and global optimization landscape of nonconvex matrix factorization," *IEEE Transactions on Information Theory*, vol. 65, no. 6, pp. 3489–3514, 2019.
- [101] E. J. Candès and B. Recht, "Exact matrix completion via convex optimization," *Foundations of Computational mathematics*, vol. 9, no. 6, p. 717, 2009.
- [102] B. Recht, M. Fazel, and P. A. Parrilo, "Guaranteed minimum-rank solutions of linear matrix equations via nuclear norm minimization," *SIAM review*, vol. 52, no. 3, pp. 471–501, 2010.
- [103] D. Park, A. Kyrillidis, C. Caramanis, and S. Sanghavi, "Non-square matrix sensing without spurious local minima via the burer-monteiro approach," *arXiv preprint arXiv:1609.03240*, 2016.
- [104] S. Bhojanapalli, B. Neyshabur, and N. Srebro, "Global optimality of local search for low rank matrix recovery," *arXiv preprint arXiv:1605.07221*, 2016.
- [105] Z. Zhu, Q. Li, G. Tang, and M. B. Wakin, "Global optimality in low-rank matrix optimization," *IEEE Transactions on Signal Processing*, vol. 66, no. 13, pp. 3614–3628, 2018.
- [106] Q. Li, Z. Zhu, and G. Tang, "The non-convex geometry of low-rank matrix optimization," *Information and Inference: A Journal of the IMA*, vol. 8, no. 1, pp. 51–96, 2018.
- [107] J. D. Rennie and N. Srebro, "Fast maximum margin matrix factorization for collaborative prediction," in *Proceedings of the 22nd international conference on Machine learning*, pp. 713–719, 2005.
- [108] Y. Koren, "The bellkor solution to the netflix grand prize," 2009.
- [109] P. Biswas, T.-C. Lian, T.-C. Wang, and Y. Ye, "Semidefinite programming based algorithms for sensor network localization," *ACM Transactions on Sensor Networks (TOSN)*, vol. 2, no. 2, pp. 188–220, 2006.
- [110] A. M.-C. So and Y. Ye, "Theory of semidefinite programming for sensor network localization," *Mathematical Programming*, vol. 109, no. 2-3, pp. 367–384, 2007.
- [111] L. Wu, A. Ganesh, B. Shi, Y. Matsushita, Y. Wang, and Y. Ma, "Robust photometric stereo via low-rank matrix completion and recovery," in *Asian Conference on Computer Vision*, pp. 703–717, Springer, 2010.
- [112] X. Zhou, C. Yang, H. Zhao, and W. Yu, "Low-rank modeling and its applications in image analysis," *ACM Computing Surveys (CSUR)*, vol. 47, no. 2, pp. 1–33, 2014.
- [113] Y. Yang, J. Ma, and S. Osher, "Seismic data reconstruction via matrix completion," *Inverse Problems & Imaging*, vol. 7, no. 4, p. 1379, 2013.
- [114] R. Kumar, C. Da Silva, O. Akalin, A. Y. Aravkin, H. Mansour, B. Recht, and F. J. Herrmann, "Efficient matrix completion for seismic data reconstruction," *Geophysics*, vol. 80, no. 5, pp. V97–V114, 2015.

- [115] E. J. Candès, X. Li, Y. Ma, and J. Wright, "Robust principal component analysis?," *Journal of the ACM (JACM)*, vol. 58, no. 3, p. 11, 2011.
- [116] Y. Peng, A. Ganesh, J. Wright, W. Xu, and Y. Ma, "Rasl: Robust alignment by sparse and low-rank decomposition for linearly correlated images," *IEEE transactions on pattern analysis and machine intelligence*, vol. 34, no. 11, pp. 2233–2246, 2012.
- [117] P. J. Huber, "Robust estimation of a location parameter," in *Breakthroughs in statistics*, pp. 492–518, Springer, 1992.
- [118] X. Li, Z. Zhu, A. Man-Cho So, and R. Vidal, "Nonconvex robust low-rank matrix recovery," *SIAM Journal on Optimization*, vol. 30, no. 1, pp. 660–686, 2020.
- [119] V. Charisopoulos, Y. Chen, D. Davis, M. Díaz, L. Ding, and D. Drusvyatskiy, "Low-rank matrix recovery with composite optimization: good conditioning and rapid convergence," *arXiv preprint arXiv:1904.10020*, 2019.
- [120] H. Xu, C. Caramanis, and S. Sanghavi, "Robust pca via outlier pursuit," in *Advances in Neural Information Processing Systems*, pp. 2496–2504, 2010.
- [121] G. Lerman and T. Maunu, "Fast, robust and non-convex subspace recovery," *Information and Inference: A Journal of the IMA*, vol. 7, no. 2, pp. 277–336, 2018.
- [122] T. Maunu, T. Zhang, and G. Lerman, "A well-tempered landscape for non-convex robust subspace recovery," *Journal of Machine Learning Research*, vol. 20, no. 37, 2019.
- [123] G. Lerman and T. Maunu, "An overview of robust subspace recovery," *Proceedings of the IEEE*, vol. 106, no. 8, pp. 1380–1410, 2018.
- [124] M. C. Tsakiris and R. Vidal, "Hyperplane clustering via dual principal component pursuit," in *International conference on machine learning*, pp. 3472–3481, PMLR, 2017.
- [125] M. C. Tsakiris and R. Vidal, "Dual principal component pursuit," *The Journal of Machine Learning Research*, vol. 19, no. 1, pp. 684–732, 2018.
- [126] Z. Zhu, Y. Wang, D. Robinson, D. Naiman, R. Vidal, and M. Tsakiris, "Dual principal component pursuit: Improved analysis and efficient algorithms," in *Advances in Neural Information Processing Systems*, pp. 2171–2181, 2018.
- [127] T. Ding *et al.*, *Subspace Learning for Data Arising from a Union of Subspaces of High Relative Dimension*. PhD thesis, Johns Hopkins University, 2021.
- [128] Y. Zhai, Z. Yang, Z. Liao, J. Wright, and Y. Ma, "Complete dictionary learning via ℓ^4 -norm maximization over the orthogonal group," *arXiv preprint arXiv:1906.02435*, 2019.
- [129] Y. Zhang, Y. Lau, H.-W. Kuo, S. Cheung, A. Pasupathy, and J. Wright, "On the global geometry of sphere-constrained sparse blind deconvolution," in *Computer Vision and Pattern Recognition (CVPR), 2017 IEEE Conference on*, pp. 4381–4389, IEEE, 2017.
- [130] X. Li, S. Chen, Z. Deng, Q. Qu, Z. Zhu, and A. M. C. So, "Nonsmooth optimization over stiefel manifold: Riemannian subgradient methods," *arXiv preprint arXiv:1911.05047*, 2019.
- [131] Y. Shen, Y. Xue, J. Zhang, K. B. Letaief, and V. Lau, "Complete dictionary learning via ℓ^p -norm maximization," 2020.
- [132] D. A. Spielman, H. Wang, and J. Wright, "Exact recovery of sparsely-used dictionaries," in *Conference on Learning Theory*, 2012.
- [133] Q. Qu, J. Sun, and J. Wright, "Finding a sparse vector in a subspace: Linear sparsity using alternating directions," in *Advances in Neural Information Processing Systems*, pp. 3401–3409, 2014.
- [134] P.-A. Absil, R. Mahoney, and R. Sepulchre, *Optimization Algorithms on Matrix Manifolds*. Princeton University Press, 2009.
- [135] N. Boumal, "An introduction to optimization on smooth manifolds." Available online, Aug 2020.
- [136] J. Wright, Y. Ma, J. Mairal, G. Sapiro, T. S. Huang, and S. Yan, "Sparse representation for computer vision and pattern recognition," *Proceedings of the IEEE*, vol. 98, no. 6, pp. 1031–1044, 2010.

- [137] M. Elad, *Sparse and redundant representations: from theory to applications in signal and image processing*. Springer Science & Business Media, 2010.
- [138] J. F. Murray and K. Kreutz-Delgado, "Learning sparse overcomplete codes for images," *Journal of VLSI signal processing systems for signal, image and video technology*, vol. 45, no. 1-2, pp. 97–110, 2006.
- [139] M. Elad and M. Aharon, "Image denoising via sparse and redundant representations over learned dictionaries," *IEEE Transactions on Image processing*, vol. 15, no. 12, pp. 3736–3745, 2006.
- [140] J. Yang, J. Wright, T. S. Huang, and Y. Ma, "Image super-resolution via sparse representation," *IEEE transactions on image processing*, vol. 19, no. 11, pp. 2861–2873, 2010.
- [141] J.-L. Starck, E. Pantin, and F. Murtagh, "Deconvolution in astronomy: A review," *Publications of the Astronomical Society of the Pacific*, vol. 114, no. 800, p. 1051, 2002.
- [142] E. A. Pnevmatikakis, D. Soudry, Y. Gao, T. A. Machado, J. Merel, D. Pfau, T. Reardon, Y. Mu, C. Lacefield, W. Yang, *et al.*, "Simultaneous denoising, deconvolution, and demixing of calcium imaging data," *Neuron*, vol. 89, no. 2, pp. 285–299, 2016.
- [143] S. C. Cheung, J. Y. Shin, Y. Lau, Z. Chen, J. Sun, Y. Zhang, M. A. Müller, I. M. Eremin, J. N. Wright, and A. N. Pasupathy, "Dictionary learning in fourier-transform scanning tunneling spectroscopy," *Nature communications*, vol. 11, no. 1, pp. 1–11, 2020.
- [144] L. Shi and Y. Chi, "Manifold gradient descent solves multi-channel sparse blind deconvolution provably and efficiently," *arXiv preprint arXiv:1911.11167*, 2019.
- [145] A. Ahmed, B. Recht, and J. Romberg, "Blind deconvolution using convex programming," *IEEE Transactions on Information Theory*, vol. 60, no. 3, pp. 1711–1732, 2014.
- [146] C. Garcia-Cardona and B. Wohlberg, "Convolutional dictionary learning: A comparative review and new algorithms," *IEEE Transactions on Computational Imaging*, vol. 4, no. 3, pp. 366–381, 2018.
- [147] T. G. Kolda and B. W. Bader, "Tensor decompositions and applications," *SIAM review*, vol. 51, no. 3, pp. 455–500, 2009.
- [148] A. Anandkumar, R. Ge, D. Hsu, S. M. Kakade, and M. Telgarsky, "Tensor decompositions for learning latent variable models," *Journal of Machine Learning Research*, vol. 15, pp. 2773–2832, 2014.
- [149] N. D. Sidiropoulos, L. De Lathauwer, X. Fu, K. Huang, E. E. Papalexakis, and C. Faloutsos, "Tensor decomposition for signal processing and machine learning," *IEEE Transactions on Signal Processing*, vol. 65, no. 13, pp. 3551–3582, 2017.
- [150] M. Janzamin, R. Ge, J. Kossaifi, and A. Anandkumar, "Spectral learning on matrices and tensors," *Foundations and Trends® in Machine Learning*, vol. 12, no. 5-6, pp. 393–536, 2019.
- [151] C. J. Hillar and L.-H. Lim, "Most tensor problems are NP-hard," *Journal of the ACM (JACM)*, vol. 60, no. 6, p. 45, 2013.
- [152] M. Sanjabi, S. Baharlouei, M. Razaviyayn, and J. D. Lee, "When does non-orthogonal tensor decomposition have no spurious local minima?," *arXiv preprint arXiv:1911.09815*, 2019.
- [153] S. Balakrishnan, M. J. Wainwright, and B. Yu, "Statistical guarantees for the em algorithm: From population to sample-based analysis," *The Annals of Statistics*, vol. 45, no. 1, pp. 77–120, 2017.
- [154] J. Xu, D. J. Hsu, and A. Maleki, "Global analysis of expectation maximization for mixtures of two gaussians," in *Advances in Neural Information Processing Systems*, pp. 2676–2684, 2016.
- [155] C. Daskalakis, C. Tzamos, and M. Zampetakis, "Ten steps of em suffice for mixtures of two gaussians," *arXiv preprint arXiv:1609.00368*, 2016.
- [156] S. Dasgupta and L. Schulman, "A probabilistic analysis of em for mixtures of separated, spherical gaussians," *Journal of Machine Learning Research*, vol. 8, no. Feb, pp. 203–226, 2007.
- [157] C. Jin, Y. Zhang, S. Balakrishnan, M. J. Wainwright, and M. I. Jordan, "Local maxima in the likelihood of gaussian mixture models: Structural results and algorithmic consequences," in *Advances in neural information processing systems*, pp. 4116–4124, 2016.

- [158] T. Bendory, R. Beinert, and Y. C. Eldar, "Fourier phase retrieval: Uniqueness and algorithms," in *Compressed Sensing and its Applications*, pp. 55–91, Springer, 2017.
- [159] A. Krizhevsky, I. Sutskever, and G. E. Hinton, "Imagenet classification with deep convolutional neural networks," in *Advances in neural information processing systems*, pp. 1097–1105, 2012.
- [160] Y. LeCun, Y. Bengio, and G. Hinton, "Deep learning," *nature*, vol. 521, no. 7553, pp. 436–444, 2015.
- [161] A. W. Senior, R. Evans, J. Jumper, J. Kirkpatrick, L. Sifre, T. Green, C. Qin, A. Židek, A. W. Nelson, A. Bridgland, *et al.*, "Improved protein structure prediction using potentials from deep learning," *Nature*, vol. 577, no. 7792, pp. 706–710, 2020.
- [162] R. Vidal, J. Bruna, R. Giryes, and S. Soatto, "Mathematics of deep learning," *arXiv preprint arXiv:1712.04741*, 2017.
- [163] R.-Y. Sun, "Optimization for deep learning: An overview," *Journal of the Operations Research Society of China*, vol. 8, no. 2, pp. 249–294, 2020.
- [164] R. Sun, D. Li, S. Liang, T. Ding, and R. Srikant, "The global landscape of neural networks: An overview," *IEEE Signal Processing Magazine*, vol. 37, no. 5, pp. 95–108, 2020.
- [165] C. Ma, S. Wojtowytsch, L. Wu, *et al.*, "Towards a mathematical understanding of neural network-based machine learning: what we know and what we don't," *arXiv preprint arXiv:2009.10713*, 2020.
- [166] J. Berner, P. Grohs, G. Kutyniok, and P. Petersen, "The modern mathematics of deep learning," *arXiv preprint arXiv:2105.04026*, 2021.
- [167] C. Fang, H. Dong, and T. Zhang, "Mathematical models of overparameterized neural networks," *Proceedings of the IEEE*, vol. 109, no. 5, pp. 683–703, 2021.
- [168] P. Baldi and K. Hornik, "Neural networks and principal component analysis: Learning from examples without local minima," *Neural networks*, vol. 2, no. 1, pp. 53–58, 1989.
- [169] M. Nouiehed and M. Razaviyayn, "Learning deep models: Critical points and local openness," *arXiv preprint arXiv:1803.02968*, 2018.
- [170] Z. Zhu, D. Soudry, Y. C. Eldar, and M. B. Wakin, "The global optimization geometry of shallow linear neural networks," *Journal of Mathematical Imaging and Vision*, pp. 1–14, 2019.
- [171] C. Yun, S. Sra, and A. Jadbabaie, "Global optimality conditions for deep neural networks," in *International Conference on Learning Representations*, 2018.
- [172] S. Arora, N. Cohen, N. Golowich, and W. Hu, "A convergence analysis of gradient descent for deep linear neural networks," *arXiv preprint arXiv:1810.02281*, 2018.
- [173] S. Arora, N. Cohen, W. Hu, and Y. Luo, "Implicit regularization in deep matrix factorization," *Advances in Neural Information Processing Systems*, vol. 32, 2019.
- [174] T. Laurent and J. Brecht, "Deep linear networks with arbitrary loss: All local minima are global," in *International conference on machine learning*, pp. 2902–2907, PMLR, 2018.
- [175] M. Janzamin, H. Sedghi, and A. Anandkumar, "Beating the perils of non-convexity: Guaranteed training of neural networks using tensor methods," *arXiv preprint arXiv:1506.08473*, 2015.
- [176] M. Mondelli and A. Montanari, "On the connection between learning two-layers neural networks and tensor decomposition," *arXiv preprint arXiv:1802.07301*, 2018.
- [177] B. D. Haeffele and R. Vidal, "Global optimality in neural network training," in *Proceedings of the IEEE Conference on Computer Vision and Pattern Recognition*, pp. 7331–7339, 2017.
- [178] S. Feizi, H. Javadi, J. Zhang, and D. Tse, "Porcupine neural networks: (almost) all local optima are global," *arXiv preprint arXiv:1710.02196*, 2017.
- [179] R. Ge, J. D. Lee, and T. Ma, "Learning one-hidden-layer neural networks with landscape design," *arXiv preprint arXiv:1711.00501*, 2017.

- [180] W. Gao, A. V. Makkuva, S. Oh, and P. Viswanath, "Learning one-hidden-layer neural networks under general input distributions," *arXiv preprint arXiv:1810.04133*, 2018.
- [181] I. Safran and O. Shamir, "Spurious local minima are common in two-layer relu neural networks," *arXiv preprint arXiv:1712.08968*, 2017.
- [182] C. Yun, S. Sra, and A. Jadbabaie, "Small nonlinearities in activation functions create bad local minima in neural networks," in *International Conference on Learning Representations*, 2018.
- [183] I. Safran and O. Shamir, "Spurious local minima are common in two-layer relu neural networks," in *International Conference on Machine Learning*, pp. 4433–4441, PMLR, 2018.
- [184] S. Liang, R. Sun, J. D. Lee, and R. Srikant, "Adding one neuron can eliminate all bad local minima," *Advances in Neural Information Processing Systems*, vol. 2018, pp. 4350–4360, 2018.
- [185] B. D. Haeffele and R. Vidal, "Global optimality in tensor factorization, deep learning, and beyond," *arXiv preprint arXiv:1506.07540*, 2015.
- [186] D. G. Mixon, H. Parshall, and J. Pi, "Neural collapse with unconstrained features," *arXiv preprint arXiv:2011.11619*, 2020.
- [187] J. Lu and S. Steinerberger, "Neural collapse with cross-entropy loss," *arXiv preprint arXiv:2012.08465*, 2020.
- [188] E. Weinan and S. Wojtowytsch, "On the emergence of tetrahedral symmetry in the final and penultimate layers of neural network classifiers," *arXiv preprint arXiv:2012.05420*, 2020.
- [189] C. Fang, H. He, Q. Long, and W. J. Su, "Exploring deep neural networks via layer-peeled model: Minority collapse in imbalanced training," *Proceedings of the National Academy of Sciences*, vol. 118, no. 43, 2021.
- [190] F. Graf, C. Hofer, M. Niethammer, and R. Kwitt, "Dissecting supervised contrastive learning," in *International Conference on Machine Learning*, pp. 3821–3830, PMLR, 2021.
- [191] T. Ergen and M. Pilanci, "Revealing the structure of deep neural networks via convex duality," in *International Conference on Machine Learning*, pp. 3004–3014, PMLR, 2021.
- [192] Z. Zhu, T. Ding, J. Zhou, X. Li, C. You, J. Sulam, and Q. Qu, "A geometric analysis of neural collapse with unconstrained features," *arXiv preprint arXiv:2105.02375*, 2021.
- [193] W. Ji, Y. Lu, Y. Zhang, Z. Deng, and W. J. Su, "An unconstrained layer-peeled perspective on neural collapse," in *International Conference on Learning Representations*, 2022.
- [194] J. Zhou, X. Li, T. Ding, C. You, Q. Qu, and Z. Zhu, "On the optimization landscape of neural collapse under mse loss: Global optimality with unconstrained features," *arXiv preprint arXiv:2203.01238*, 2022.
- [195] G. Cybenko, "Approximation by superposition of sigmoidal functions," *Mathematics of Control, Signals and Systems*, vol. 2, no. 4, pp. 303–314, 1989.
- [196] K. Hornik, "Approximation capabilities of multilayer feedforward networks," *Neural networks*, vol. 4, no. 2, pp. 251–257, 1991.
- [197] Z. Lu, H. Pu, F. Wang, Z. Hu, and L. Wang, "The expressive power of neural networks: a view from the width," in *Proceedings of the 31st International Conference on Neural Information Processing Systems*, pp. 6232–6240, 2017.
- [198] U. Shaham, A. Cloninger, and R. R. Coifman, "Provable approximation properties for deep neural networks," *Applied and Computational Harmonic Analysis*, vol. 44, no. 3, pp. 537–557, 2018.
- [199] V. Pappayan, X. Han, and D. L. Donoho, "Prevalence of neural collapse during the terminal phase of deep learning training," *Proceedings of the National Academy of Sciences*, vol. 117, no. 40, pp. 24652–24663, 2020.
- [200] X. Han, V. Pappayan, and D. L. Donoho, "Neural collapse under MSE loss: Proximity to and dynamics on the central path," in *International Conference on Learning Representations*, 2022.
- [201] T. Tirer and J. Bruna, "Extended unconstrained features model for exploring deep neural collapse," *arXiv preprint arXiv:2202.08087*, 2022.

- [202] D. Soudry, E. Hoffer, M. S. Nacson, S. Gunasekar, and N. Srebro, "The implicit bias of gradient descent on separable data," *The Journal of Machine Learning Research*, vol. 19, no. 1, pp. 2822–2878, 2018.
- [203] C. You, Z. Zhu, Q. Qu, and Y. Ma, "Robust recovery via implicit bias of discrepant learning rates for double over-parameterization," *Advances in Neural Information Processing Systems*, vol. 33, pp. 17733–17744, 2020.
- [204] S. Liu, Z. Zhu, Q. Qu, and C. You, "Robust training under label noise by over-parameterization," *arXiv preprint arXiv:2202.14026*, 2022.
- [205] E. Candes and J. Romberg, "Sparsity and incoherence in compressive sampling," *Inverse Problems*, vol. 23, no. 3, p. 969, 2007.
- [206] E. J. Candès, J. K. Romberg, and T. Tao, "Stable signal recovery from incomplete and inaccurate measurements," *Communications on Pure and Applied Mathematics*, vol. 59, no. 8, pp. 1207–1223, 2006.
- [207] E. J. Candès and T. Tao, "The power of convex relaxation: Near-optimal matrix completion," *IEEE Transactions on Information Theory*, vol. 56, no. 5, pp. 2053–2080, 2010.
- [208] T. Rapcsák and T. Csendes, "Nonlinear coordinate transformations for unconstrained optimization ii. theoretical background," *Journal of Global Optimization*, vol. 3, no. 3, pp. 359–375, 1993.
- [209] R. L. Bishop and B. O'Neill, "Manifolds of negative curvature," *Transactions of the American Mathematical Society*, vol. 145, pp. 1–49, 1969.
- [210] S.-T. Yau, "Non-existence of continuous convex functions on certain riemannian manifolds," *Mathematische Annalen*, vol. 207, no. 4, pp. 269–270, 1974.
- [211] B. Barak, J. A. Kelner, and D. Steurer, "Dictionary learning and tensor decomposition via the sum-of-squares method," in *Proceedings of the forty-seventh annual ACM symposium on Theory of computing*, pp. 143–151, 2015.
- [212] S. Boyd and L. Vandenberghe, *Convex optimization*. Cambridge university press, 2004.
- [213] D. Davis, D. Drusvyatskiy, K. J. MacPhee, and C. Paquette, "Subgradient methods for sharp weakly convex functions," *Journal of Optimization Theory and Applications*, vol. 179, no. 3, pp. 962–982, 2018.
- [214] D. Davis and D. Drusvyatskiy, "Graphical convergence of subgradients in nonconvex optimization and learning," *arXiv preprint arXiv:1810.07590*, 2018.
- [215] Y. Bai, Q. Jiang, and J. Sun, "Subgradient descent learns orthogonal dictionaries," in *7th International Conference on Learning Representations, ICLR 2019*, 2019.
- [216] V. Charisopoulos, D. Davis, M. Díaz, and D. Drusvyatskiy, "Composite optimization for robust blind deconvolution," *arXiv preprint arXiv:1901.01624*, 2019.
- [217] L. Ding, L. Jiang, Y. Chen, Q. Qu, and Z. Zhu, "Rank overspecified robust matrix recovery: Subgradient method and exact recovery," *arXiv preprint arXiv:2109.11154*, 2021.
- [218] R. T. Rockafellar and R. J.-B. Wets, *Variational analysis*, vol. 317. Springer Science & Business Media, 2009.
- [219] C. Criscitiello and N. Boumal, "Efficiently escaping saddle points on manifolds," in *Advances in Neural Information Processing Systems*, pp. 5987–5997, 2019.
- [220] Y. Sun, N. Flammarion, and M. Fazel, "Escaping from saddle points on riemannian manifolds," in *Advances in Neural Information Processing Systems*, pp. 7276–7286, 2019.
- [221] S. S. Du, C. Jin, J. D. Lee, M. I. Jordan, A. Singh, and B. Poczos, "Gradient descent can take exponential time to escape saddle points," in *Advances in neural information processing systems*, pp. 1067–1077, 2017.
- [222] Y. Chen, Y. Chi, J. Fan, and C. Ma, "Gradient descent with random initialization: Fast global convergence for nonconvex phase retrieval," *Mathematical Programming*, pp. 1–33, 2018.

A Critical Points of Low Rank Matrix Factorization

In this appendix, we give a more detailed accounting of the critical points of two model matrix factorization problems.

Symmetric Low Rank Matrix Factorization We begin by considering the symmetric factorization problem (2.16). This is a nonconvex optimization problem, with orthogonal symmetry $U \equiv U\Gamma$. As we will see, its critical points can be described in terms of the eigendecomposition of the symmetric matrix X_0 . Here, X_0 has a complete orthonormal basis of eigenvectors ξ_1, \dots, ξ_n , with corresponding nonnegative eigenvalues $\lambda_1 > \lambda_2 > \dots > \lambda_r > \lambda_{r+1} = \dots = \lambda_n = 0$.²⁸ In other words, we can write

$$X_0 = \sum_i \lambda_i \xi_i \xi_i^*. \quad (\text{A.1})$$

Using properties of the eigenvectors, it is not difficult to show that every optimal factorization $X_0 = UU^*$ can be written as

$$U = \left[\lambda_1^{1/2} \xi_1 \mid \dots \mid \lambda_r^{1/2} \xi_r \right] \Gamma, \quad (\text{A.2})$$

for some orthogonal matrix $\Gamma \in O(r)$. By setting $\nabla\varphi = \mathbf{0}$, we can obtain the following characterization of critical points: U is a critical point if and only if it can be written as

$$U = [\phi_1 \mid \phi_2 \mid \dots \mid \phi_r] \Gamma, \quad \Gamma \in O(r), \quad (\text{A.3})$$

where the columns ϕ_j ($1 \leq j \leq r'$, $r' \leq r$) are generated by appropriately scaling some orthogonal eigenvector of X_0 , so that

$$\phi_1 = \lambda_{i_1}^{1/2} \xi_{i_1}, \dots, \phi_{r'} = \lambda_{i_{r'}}^{1/2} \xi_{i_{r'}}, \quad (\text{A.4})$$

with the indices $\{i_1, i_2, \dots, i_{r'}\} \subseteq [r]$, and setting any remaining ϕ_ℓ to $\mathbf{0}$. In words, equivalence classes of critical points are generated by selecting subsets of the eigenvectors of X_0 . Selecting the r leading eigenvectors, as in (A.2), gives a global minimizer. The curvature at other critical points can be studied through the Hessian

$$\nabla^2\varphi[\mathbf{W}, \mathbf{W}] = \frac{1}{2} \|U\mathbf{W}^* + \mathbf{W}U^*\|_F^2 + \langle U\mathbf{U}^* - \mathbf{Y}, \mathbf{W}\mathbf{W}^* \rangle. \quad (\text{A.5})$$

Evaluating this at critical points, and using orthogonality of the eigenvectors ξ_i , we can observe that:

- *Saddle points* occur at any critical point \bar{U} that is not generated by choosing r lead eigenvectors. Suppose that $\bar{U} = \Phi\Gamma$, and $\phi_\ell = \mathbf{0}$ for some $\ell > r$. Then there is some lead eigenvector $\pm\xi_i$ ($i \leq r$) which does not participate in Φ . Consider a perturbation $\pm\mathbf{W} = \xi_i e_\ell^* \Gamma$ which moves ϕ_ℓ in the direction of the neglected eigenvector ξ_i or its negative. The second derivative of φ in this direction is simply

$$\nabla^2\varphi[\mathbf{W}, \mathbf{W}] = \langle U\mathbf{U}^* - \mathbf{Y}, \xi_i \xi_i^* \rangle = -\lambda_i < 0. \quad (\text{A.6})$$

In words: the objective function exhibits strict negative curvature in any direction that perturbs any zero column ϕ_ℓ in the direction of a neglected. This is intuitive, since this modification allows the approximation to capture more of the energy of the observation \mathbf{Y} . Because we can perturb in either the direction of $+\xi_\ell$ or $-\xi_\ell$, this can be interpreted as negative curvature in a direction that breaks this symmetry.

- *Local minimizers* occur only at the global minimizers, of the form (A.2). There is a manifold of local minimizers, isometric to $O(r)$. This generalizes the “circle” of local minimizers observed in phase retrieval.

²⁸For simplicity, we assume that the nonzero eigenvalues are distinct. Problems with repeated eigenvalues exhibit a similar structure, with minor modifications.

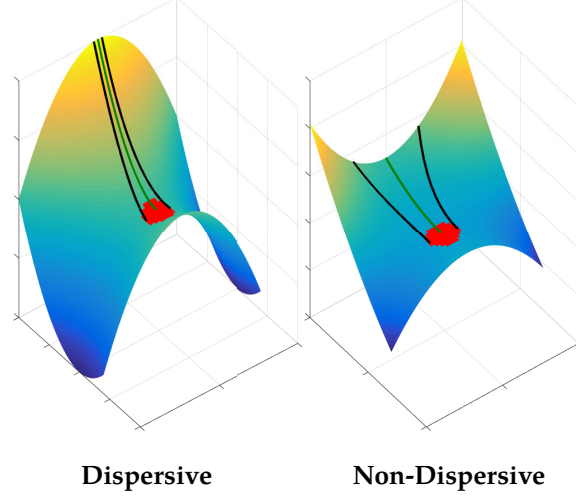


Figure 10: Dispersive and Non-dispersive Flows. Left: Dispersive functions exhibit global negative curvature. Right: nondispersive functions may exhibit positive curvature upstream of a saddle. In this situation, randomly initialized gradient descent may stagnate near the saddle point.

General Low Rank Matrix Factorization In comparison to symmetric matrix factorization, the problem of factorizing a general rectangular matrix

$$\mathbf{X} = \mathbf{U}\mathbf{V}^*, \quad \mathbf{U} \neq \mathbf{V} \quad (\text{A.7})$$

admits a full generalized linear symmetry. As mentioned above, this can be reduced to an orthogonal symmetry, by introducing an additional penalty, solving

$$\min_{\mathbf{U}, \mathbf{V}} \varphi(\mathbf{U}, \mathbf{V}) + \rho_s(\mathbf{U}, \mathbf{V}). \quad (\text{A.8})$$

For example, setting $\rho_s(\mathbf{U}, \mathbf{V}) = \|\mathbf{U}^*\mathbf{U} - \mathbf{V}^*\mathbf{V}\|_F^2$ achieves this.²⁹

How does this penalized problem behave? The critical points of this more general model also admit a simple description in terms of the spectral structure of the target matrix \mathbf{X}_0 , given by the singular value decomposition $\mathbf{X}_0 = \sum_i \sigma_i \boldsymbol{\xi}_i \boldsymbol{\nu}_i^*$. Where in the symmetric case, critical points are generated by selecting subsets of eigenvectors, here every critical point (\mathbf{U}, \mathbf{V}) is generated by selecting subsets of *singular* vectors:

$$\mathbf{U} = [\phi_1 | \cdots | \phi_r] \mathbf{\Gamma} \quad (\text{A.9})$$

$$\mathbf{V} = [\zeta_1 | \cdots | \zeta_r] \mathbf{\Gamma}, \quad \mathbf{\Gamma} \in O(r), \quad (\text{A.10})$$

where

$$\phi_1 = \sigma_{i_1}^{1/2} \boldsymbol{\xi}_{i_1}, \dots, \phi_{r'} = \sigma_{i_{r'}}^{1/2} \boldsymbol{\xi}_{i_{r'}}, \quad (\text{A.11})$$

$$\zeta_1 = \sigma_{i_1}^{1/2} \boldsymbol{\nu}_{i_1}, \dots, \zeta_{r'} = \sigma_{i_{r'}}^{1/2} \boldsymbol{\nu}_{i_{r'}}, \quad (\text{A.12})$$

and any remaining columns ϕ_ℓ, ζ_ℓ are zero. This generalizes in a straightforward way the characterization for symmetric matrices above. Similar considerations show negative curvature in directions $\pm (\boldsymbol{\xi}_i e_\ell^*, \boldsymbol{\nu}_i e_\ell^*)$ that swap in a leading singular vector pair.

B Dispersive Structure: Negative Curvature

In this appendix, we describe in more detail the notion of *dispersion* illustrated in Figures 7, 8 and 9 and the associated critical point diagrams. This notion seems to be important for explaining why the symmetric

²⁹Other penalties are also possible – e.g., $\rho_s(\mathbf{U}, \mathbf{V}) = \|\mathbf{U}\|_F^2 + \|\mathbf{V}\|_F^2$, which encourages the factors to be balanced. This penalty is tightly connected to nuclear norm regularization.

functions encountered in this paper are amenable to simple iterative methods such as randomly initialized gradient descent. The key intuition is that these functions exhibit a global negative curvature structure. This structure can be described most cleanly in terms of a continuous-time gradient flow

$$\dot{\mathbf{x}}_t = -\nabla\varphi(\mathbf{x}_t). \quad (\text{B.1})$$

We say that two critical points \mathbf{x}^\uparrow and \mathbf{x}^\downarrow are linked by gradient flow if there is a unique integral curve \mathbf{x}_t of this differential equation, with $\lim_{t \rightarrow \infty} \mathbf{x}_t = \mathbf{x}^\downarrow$ and $\lim_{t \rightarrow -\infty} \mathbf{x}_t = \mathbf{x}^\uparrow$.

We are interested in understanding whether gradient descent tends to stagnate near \mathbf{x}^\downarrow . To this end, it is useful to study the effect of perturbations \mathbf{v}_t about \mathbf{x}_t . In particular, we are interested in understanding the behavior of the integral curve passing through $\mathbf{x}_t + \varepsilon\mathbf{v}_t$, for ε small. Under gradient flow the perturbation evolves according to the linear time varying dynamical system

$$\dot{\mathbf{v}}_t = -\nabla^2\varphi(\mathbf{x}_t)\mathbf{v}_t. \quad (\text{B.2})$$

This differential equation provides a means of tracking the effect of perturbations across time. For any $t, t' \in (-\infty, \infty)$, we can define a transport operator $T_{t,t'}$ from the tangent space at \mathbf{x}_t to the tangent space at $\mathbf{x}_{t'}$, by letting $T_{t',t}\mathbf{w}$ be the unique solution $\mathbf{v}_{t'}$ to the differential equation (B.2) with initial condition $\mathbf{v}_t = \mathbf{w}$.

The geometry of φ around the saddle point \mathbf{x}^\downarrow can be studied through the Hessian $\nabla^2\varphi(\mathbf{x}^\downarrow)$. We say that the function φ is *dispersive* along the path $\mathbf{x}^\uparrow \rightarrow \mathbf{x}^\downarrow$ if for every eigenvector \mathbf{v} of $\nabla^2\varphi(\mathbf{x}^\downarrow)$ that corresponds to a negative eigenvalue, and every $t_\uparrow \in (-\infty, \infty)$, there exists a t_\downarrow such that for every $t_\uparrow \leq t' \leq t_\downarrow < t$, $\mathbf{w} = T_{t',t}\Pi_{\mathbf{x}_t, \mathbf{x}^\downarrow}\mathbf{v}$ is a direction of negative curvature, i.e., $\mathbf{w}^*\nabla^2\varphi(\mathbf{x}_{t'})\mathbf{w} < 0$.

This somewhat cumbersome technical definition exists to capture the idea that *downstream negative curvature directions are the images of upstream negative curvature directions under gradient flow*. All of the symmetric functions studied in this paper exhibit this property. However, worst case strict saddle functions such as the ‘‘octopus function’’ [221] do not. Intuitively speaking, this negative curvature structure helps gradient descent to avoid stagnating near saddle points. This intuition has been made formal in a number of special cases: generalized phase retrieval, complete dictionary learning, and multichannel deconvolution, etc.